HHS Public Access

Author manuscript

Nat Neurosci. Author manuscript; available in PMC 2018 May 02.

Published in final edited form as:

Nat Neurosci. 2017 August ; 20(8): 1085–1095. doi:10.1038/nn.4580.

Modality-specific sensory integration and neuropeptide-mediated feedback facilitate mechano-nociceptive behavior in *Drosophila*

Chun Hu[1,3], **Meike Petersen**[1,3], **Nina Hoyer**[1,3], **Bettina Spitzweck**[1], **Federico Tenedini**[1], **Denan Wang**[1], **Alisa Gruschka**[1], **Lara S. Burchardt**[1], **Emanuela Szpotowicz**[1], **Michaela Schweizer**[1], **Ananya R. Guntur**[2], **Chung-Hui Yang**[2], and **Peter Soba**[1,4]

[1]Center for Molecular Neurobiology (ZMNH), University Medical Center Hamburg-Eppendorf, University of Hamburg, Hamburg, Germany

[2]Department of Neurobiology, Duke University Medical Center, Durham, North Carolina, U.S.A

Abstract

Nociception is an evolutionary conserved mechanism to encode and process harmful environmental stimuli. Like most animals, *Drosophila* larvae respond to a variety of nociceptive stimuli, including noxious touch and temperature, with a stereotyped escape response through activation of multimodal nociceptors. How behavioral responses to these different modalities are processed and integrated by the downstream network remains poorly understood. By combining transsynaptic labeling, ultrastructural analysis, calcium imaging, optogenetic and behavioral analyses, we uncovered a circuit specific for mechano- but not thermo-nociception. Interestingly, integration of mechanosensory input from innocuous and nociceptive sensory neurons is required for robust mechano-nociceptive responses. We further show that neurons integrating mechanosensory input facilitate primary nociceptive output via releasing short Neuropeptide F (sNPF), the *Drosophila* Neuropeptide Y (NPY) homolog. Our findings unveil how integration of somatosensory input and neuropeptide-mediated modulation can produce robust modality-specific escape behavior.

Introduction

Sensing noxious stimuli and responding with appropriate nociceptive responses is essential for avoiding potentially harmful environments[1–3]. The somatosensory system of vertebrates and invertebrates features distinct neuronal subtypes sensing different modalities (e.g. innocuous or nociceptive touch, temperature) and conveys converging and diverging

[4]corresponding author: peter.soba@zmnh.uni-hamburg.de.

[3]These authors contributed equally to this study

Contributions

The study was designed by C.H., N.H. and P.S., and directed and coordinated by P.S. Morphological analyses were performed by C.H., M.P., B.S., F.T. and A.G. The behavioral experiments were performed by C.H., N.H., M.P, B.S., F.T., and L.S.B. Calcium imaging was performed by C.H. EM analysis was performed by D.W., F.T, E.S., and M.S. Transgenic lines were generated by M.P., A.R.G. and C.H.Y. The manuscript was prepared by P.S. with input from all authors.

information to higher brain centers. This requires a multi-layered hierarchical neuronal network that reliably detects and integrates innocuous or nociceptive stimuli and translates them into appropriate behavioral responses. Moreover, neuromodulation by neuropeptides may add additional complexity to somatosensory information processing in both vertebrates and invertebrates, either by acting locally as co-neurotransmitters or globally via widespread tonic release[4–7]. In *Drosophila*, over 40 neuropeptides and corresponding G protein-coupled neuropeptide receptors have been identified so far and shown to regulate various behaviors including thermo-nociceptive sensitisation[7,8]. How different somatosensory modalities are integrated at the circuit level and modulated by neuropeptide signaling to affect nociceptive behavior is thus of great interest.

The *Drosophila* larval peripheral nervous system (PNS) provides a genetically tractable model to address these questions. It features type l ciliated neurons (chordotonal and external sensory neurons)[9], bipolar (bd) and four classes of dendritic arborization (da) neurons (C1da-C4da)[10,11]. While C2da and C3da neurons respond to innocuous touch[12,13], C4da neurons are multimodal nociceptors responding to harsh mechanical touch, noxious temperatures[14–20] and strong UV and blue light[21]. Nociceptive stimuli or optogenetic activation of C4da neurons in *Drosophila* larvae elicit a nocifensive response characterized by stereotyped rolling behavior followed by locomotion speedup[22,23]. The role of C4da neurons as primary nociceptors is well established, yet the complexity of their downstream circuitry has just started to emerge[24]. An extensive hierarchical network was found to integrate nociceptive and high-frequency vibration cues which enhance nociceptive behavioral responses. Indeed, most natural stimuli elicit multisensory responses that enhance the selection of specific behaviors[25–27]. However, it is still elusive how the network processes modality-specific sensory input to produce stimulus-dependent actions.

Here we identified novel nociceptive network components and a neuromodulatory feedback mechanism specifically required for C4da neuron-mediated mechano-nociceptive responses.

Results

A08n neurons are synaptically connected to C4da neurons

We identified downstream targets of C4da neurons by generating new Gal4 insertion lines using the InSITE (Integrase Swappable In vivo Targeting Element) system[28]. One line labeled neurons that project in close proximity to C4da axon terminals (*6.14.3-Gal4*, Supplementary Fig. 1a). Flipase (Flp)-mediated single cell labeling revealed that *6.14.3-Gal4* labeled two interneurons with cell bodies located in abdominal segment 8 forming a dense network of processes mirroring the ladder-like structure of C4da axon terminals in the VNC (Fig. 1a-a”, Supplementary Fig. 1b). Each of the two neurons forms a contra-lateral projection with ipsi- and contralateral arborizations overlapping with C4da terminals. A dorsal axonal projection terminates in the gnathal ganglia (GNG). Interestingly, these neurons were identical to A08n neurons (Supplementary Fig. 1c), which are labeled by a line (*82E12-Gal4*) found in an activation screen for nociceptive behavior[23]. We next used an intersectional split-Gal4 approach to limit Gal4-dependent gene expression to A08n and two weakly labeled anterior CNS neurons (Supplementary Fig. 1d).

We investigated the compartmentalization of A08n neurons using transgenes that specifically label presynaptic active zones (Brp-short-mCherry) or postsynaptic specializations (Dα7-GFP) together with an anti-Fas3 antibody which visualizes C2da, C3da and C4da neuron terminals. Expression in A08n neurons revealed that Dα7-GFP specifically labeled punctate structures co-localizing with the innermost Fas3 labeled fascicle, the C4da terminals (Fig. 1b, b'). Conversely, Brp signals did not overlap with C4da axon terminals, but labeled the A08n axon terminating in the GNG (Fig. 1b,b").

We next tested if presynaptic active zones of C4da neurons are in apposition to postsynaptic specializations of A08n neurons. To this end, we specifically expressed Brp-short-mCherry in C4da neurons and Dα7-GFP in A08n neurons and found that that it was indeed the case (Fig. 1c,c', Supplementary Fig. 1e,f). To further corroborate the existence of synaptic contact between A08n and C4da neurons, we delivered split-GFP-tagged Synaptobrevin (Syb-GRASP)[29] to the synaptic surface for GFP reconstitution in an activity-dependent manner and indeed detected reconstituted GFP punctae localized along the entire C4da neuron axon ladder (Fig. 1d,d', Supplementary Fig. 1g).

Finally, we expressed the presynaptic marker Rab3-GFP in C4da neurons (*trpA1-QF>rab3-GFP*) and membrane-bound GFP in A08n neurons to obtain distinguishable compartmental labeling using immuno-electron microscopy (EM, Fig. 1e). In the ventromedial neuropil of VNC cross-sections we could identify synaptic contacts of Diaminobenzidine (DAB)-labelled presynaptic vesicles of C4da neurons with postsynaptic membrane compartments of A08n neurons (Fig. 1f,f'). Semi-quantitative analyses of EM sections showed that ~28% of C4da neuron presynapses are connected to A08n neurons (57/203 C4da presynapses, n=2). Taken together, our data show that A08n neurons receive extensive direct synaptic input from C4da neurons.

DP-ilp7 neurons are connected to multiple sensory neuron subtypes

Subsequently, we also identified two insulin-like peptide 7 (ilp7)-producing neurons located in the first abdominal segment (dorsal pair (DP)-ilp7)[30], which extend neurites overlapping with C4da axon terminals (Supplementary Fig. 2a). Single cell labeling showed that DP-ilp7 neurons span the entire VNC with ipsilateral neurites forming a loose network around Fas3-labeled sensory axon terminals and additional ventro-lateral branches within the abdominal segments (Fig. 2a, Supplementary Fig. 2b,b',c). The dorsal axon of DP-ilp7 projects to the *pars intercerebralis* (PI) region in the brain lobes.

The arborization pattern of DP-ilp7 in the ventral neuropil suggested that they might not only receive input from C4da, but also from C2da or C3da neurons, which form laminated terminal projections adjacent to C4da terminals[31]. We therefore investigated the compartmental organization of DP-ilp7 and found that, similarly to A08n neurons, Dα7 but not Brp labeled the fine neurites and ventro-lateral branches projecting within the sensory terminal region, showing that these structures are likely dendrites (Fig. 2b,b"). Most of the postsynaptic Dα7 puncta were found surrounding the Fas3 labeled axons (Fig. 2b", Supplementary Fig. 2d,d') indicating input from multiple subtypes of sensory neurons. In contrast, Brp signals was restricted to the major DP-ilp7 neurite with strong axonal labeling extending anteriorly into the PI (Fig. 2 b,b', Supplementary Fig. 2d). Using Syb-GRASP we

also detected reconstituted GFP between C4da and DP-ilp7 neurons that strongly suggests direct synaptic contact (Fig. 2c,c', Supplementary Fig. 2e). To test if DP-ilp7 neurons receive additional synaptic input from other sensory neurons we used a da neuron-specific driver (*21-7-Gal4*) and indeed found specific GFP reconstitution along lateral and medial DP-ilp7 dendrites (Fig. 2d,d', Supplementary Fig. 2e). Interestingly, C2da neurons possess unique ventrolateral projections[31] (Supplementary Fig. 2c,f) suggesting them to be in contact with lateral dendrites of DP-ilp7 neurons. We also tested a C3da neuron-specific line (*nompC-Gal4*) but could not detect Syb-GRASP signals with DP-ilp7 neurons despite close apposition of C3da sensory terminals and DP-ilp7 dendrites (data not shown). These data suggest that DP-ilp7 neurons receive synaptic input from distinct classes of sensory neurons such as C4da and C2da neurons.

To corroborate these findings we performed immuno-EM by DAB-labeling of Brp-short-mCherry expressed in sensory da neurons and membrane-bound CD4-tdTomato in DP-ilp7 neurons (Fig. 2e,f). We found active zones of da neurons both on ventro-lateral as well as –medial DP-ilp7 projections closest to the midline confirming that da neurons form synaptic contacts with DP-ilp7 (Fig. 2f',f"). These findings show that DP-ilp7 neurons receive direct sensory input, likely at least from C2da and C4da neurons.

A08n respond to C4da neuron activation and are necessary for nociceptive behavior

To corroborate A08n and DP-ilp7 neurons as novel components of the nociceptive circuit, we first tested the functional relevance of A08n neurons. We optogenetically activated C4da neurons with CsChrimson[32] while monitoring calcium responses in A08n neurons with GCaMP6m in live larval preparations. A08n neurons but not local interneurons (Ln, labeled by *6.14.3-Gal4*) showed robust calcium responses after optogenetic activation of C4da neurons (Fig. 3a,b, Supplementary video 1).

To examine if A08n neurons respond to mechano-nociceptive stimulation we used a 45 mN *von Frey* filament, which was also able to elicit C4da neuron-dependent nociceptive behavior (see Fig. 3c). Mechanical stimulation of an intact abdominal segment (a4 or a5) in our preparations resulted in A08n responses comparable to optogenetic C4da activation (Fig. 3a,a'). These results confirmed that A08n are functionally connected to C4da neurons and able to respond to mechano-nociceptive stimuli.

We next assessed whether A08n neurons play a role in nociceptive behavior. C4da neurons have been shown to mediate nociceptive responses to mechanical stimuli by eliciting rolling behavior[14,15,22]. We stimulated abdominal segments (a4 or a5) of each animal twice within 2 s using a *von Frey* filament (45 mN). Interestingly, nociceptive response rates were low after the 1st stimulus and strongly increased after the 2nd stimulus, suggesting that the nocifensive response is sensitized after multiple stimulations (Fig. 3c). We observed both rolling and C-shaped body bending without execution of a complete roll (termed "bending"). Both responses were virtually abolished in animals lacking *TrpA1* receptor function, which is required for C4da-dependent mechano-nociception (Fig. 3c)[16].

To test if A08n neurons are required for nociceptive behavior we used the inwardly rectifying potassium channel Kir2.1 to hyperpolarize C4da neurons[33]. Kir2.1 expression in

C4da neurons strongly decreased mechano-nociceptive behavior, in particular larval rolling (Fig. 3c). Similarly, Kir2.1 expression in A08 neurons caused a significant reduction in nociceptive responses, but did not affect innocuous touch or locomotion behavior (Fig. 3c, Supplementary Fig. 3a,b). These results show that A08n activity is required for mechano-nociceptive behavior.

Activation of A08n but not DP-ilp7 neurons is sufficient for nociceptive behavior

We next addressed whether A08n or DP-ilp7 neurons are sufficient to elicit nociceptive behavioral responses. To this end we expressed CsChrimson in C4da, A08n or ilp7 neurons, which permits optogenetic activation with long-wavelength light invisible to larvae (>600nm). Activation of C4da neurons by CsChrimson resulted in robust induction of nociceptive rolling and escape responses (Fig. 3d, Supplementary video 2). Of note however, strong CsChrimson expression with *ppk-Gal4* but not *27H06-LexA* or any other lines used resulted in partial degeneration of C4da neurons (Supplementary Fig. 4a,b). Activation of CsChrimson expressing A08n neurons was sufficient to induce nociceptive responses (Fig. 3d, Supplementary video 3). Most animals displayed rolling and escape behavior immediately after light induction, completely recapitulating C4da neuron dependent nociceptive behaviors. We confirmed that rolling behavior was specifically linked to A08n using Flip-out experiments, which showed an exclusive correlation between CsChrimson expression in A08n and rolling behavior (Supplementary Fig. 4c–f). In contrast, optogenetic activation of ilp7 neurons did not induce larval rolling (Fig. 3d).

We then tested if inhibition of A08n or ilp7 neurons could suppress nociceptive behavior induced by optogenetic activation of C4da neurons. Expression of Kir2.1 in A08n or ilp7 neurons reduced C4da neuron induced rolling behavior. Particularly, A08n neuron silencing resulted in strong suppression of nociceptive responses not further enhanced by ilp7 neuron inhibition (Fig. 3e). Conversely, inhibition of C4da or ilp7 neurons did not affect rolling behavior induced by optogenetic activation of A08n neurons (Supplementary Fig. 4g,h) suggesting that C4da and ilp7 neurons both act upstream of A08n neurons. We also tested a possible direct connection between A08n and DP-ilp7 neurons using Syb-GRASP and calcium imaging. While we could detect low levels of specific GFP reconstitution from A08n onto DP-ilp7 neurons (Supplementary Fig. 4i–k)), neither optogenetic activation of A08n nor ilp7 neurons elicited calcium responses in the corresponding subset (Supplementary Fig. 4l).

Our results show that A08n neurons are necessary and sufficient for nociceptive behavioral responses downstream of C4da neurons. Ilp7 neurons, however, are not sufficient to induce nociceptive behavior, but play a modulatory role downstream of C4da and upstream of A08n neurons.

DP-ilp7 neurons facilitate mechano-nociceptive behavior

To address a possible modulatory link between DP-ilp7 neuron and nociception, we first tested how ilp7 neuron activity affects mechano-nociceptive behavior. Interestingly, ilp7 neuron inactivation by Kir2.1 but not Tetanus toxin light chain (TnT) resulted in strong suppression of mechano-nociceptive responses, which indicates that excitability but not

synaptic transmission is required for their function in this paradigm (Fig. 4a). Consistently, Kir2.1-mediated silencing using a DP-ilp7 neuron-specific line similarly inhibited mechano-nociceptive responses (Fig. 4a, Supplementary Fig. 5a). Ilp7 neuron silencing did not impair innocuous touch behavior (Supplementary Fig. 3b) suggesting that DP-ilp7 neuron function is specifically required for nociception.

To test if DP-ilp7 neuron function can also facilitate mechano-nociceptive responses we used CsChrimson mediated activation during *von Frey* filament stimulation. Strikingly, acute optogenetic activation of ilp7 or DP-ilp7 neurons strongly enhanced nociceptive response rates already after the 1st stimulus (Fig. 4b). Enhanced mechano-nociceptive behavior strictly depended on CsChrimson activation as behavioral responses under low light conditions were indistinguishably from control animals suggesting that DP-ilp7 neuron activity is necessary and strongly facilitates mechano-nociceptive responses, thus exerting bimodal control on nociceptive behavior.

DP-ilp7 neuron activation scales with multisensory input

Based on the modulatory role DP-ilp7 neurons in nociceptive behavior we suspected that their function is linked to their multisensory input. We used larval preparations expressing CsChrimson in subsets of sensory neurons and monitored calcium responses in DP-ilp7 neurons. Activation of C1da/bd, C3da or C4da neurons (*ppk-Gal4* or *27H06-LexA*) did not yield significant responses in DP-ilp7 neurons (Fig. 4c,c' and data not shown). However, optogenetic activation of C2da neurons labeled by a newly identified line (*R78A01-Gal4*, Supplementary Fig. 5b,b') was sufficient to elicit DP-ilp7 neuron responses (Fig. 4c,c'). Our findings on DP-ilp7 neuron connectivity prompted us to test if DP-ilp7 neuron responses could scale with additional synaptic input. To this end, we co-activated C2da neurons together with C3da and/or C4da neurons and found that DP-ilp7 activation was indeed significantly increased with the addition of each class (Fig. 4c,c'). While C3da or C4da neurons were not sufficient for DP-ilp7 activation, calcium responses were nonetheless significantly enhanced in a stepwise manner by multisensory activation of C2-4da neurons (Fig. 4c', Supplementary video 4). Additional activation of C1da/bd neurons did not increase DP-ilp7 neuron responses suggesting they are not involved in this circuit. These findings show that besides C2da neurons, C3da and C4da but not C1da neurons are functionally connected to DP-ilp7 neurons and contribute to their full activation. We also observed strong DP-ilp7 neuron activation after mechano-nociceptive stimulation, to a comparable extent as optogenetic activation of C2-C4da neurons (Fig. 4c,c'). We did not observe significant activation of other ilp7 neurons except for already described spontaneous and stimulus independent activity of the two most posterior neurons (data not shown)[34].

Our results show that DP-ilp7 neurons respond to mechanosensory input via C2da neurons, and calcium responses scale with additional sensory input from C3da and C4da neurons.

Innocuous touch neuron function is required for mechano-nociceptive behavior and partially integrated by DP-ilp7 neurons

As innocuous touch neurons (C2da and C3da) are functionally integrated into the nociceptive circuit via DP-ilp7 neurons, we hypothesized that multisensory integration of

mechanosensory da neuron input might play a crucial role for nociceptive responses. To test the impact of each subset, we first inactivated C2da, C3da, or both subtypes by expressing Kir2.1 or TnT and analyzed mechano-nociceptive responses. Strikingly, larval rolling was strongly impaired when we silenced C2da or C3da neurons (Fig. 4d, Supplementary Fig. 5c,d). C3da but not C2da neuron inhibition additionally impaired innocuous touch responses (Supplementary Fig. 5e). These results show that C2da and C3da neurons play an essential role in mechano-nociception.

As C2da neuron dependent behaviors have not been extensively examined before, we tested their optogenetically-induced responses. Surprisingly, C2da neuron activation resulted in continuous rolling of C-shaped animals without writhing or locomotion speedup observed for C4da neuron activation[23,35] (Fig. 4e, Supplementary video 5). We excluded any co-activation of C4da neurons by using *ppk-Gal80* to suppress Gal4 expression of *R78A01-Gal4* in occasionally labeled posterior and thoracic C4da neurons (Supplementary Fig. 5b and data not shown). In contrast, C3da neuron activation resulted in larval contraction as previously described (Fig. 4e, Supplementary video 6)[22,36]. Interestingly, C2da neuron rolling behavior was partially dependent on ilp7 neuron function (Fig. 4f) suggesting that they integrate aspects of C2da and C4da neuron dependent behaviors.

Taken together, activity of innocuous touch neurons (C2da and C3da) is necessary for mechano-nociceptive responses and C2da neuron dependent C-shaped bending and rolling is partially dependent on ilp7 neuron function.

sNPF localizes to DP-ilp7 dendrites and is required for nociceptive behavior

The puzzling result that silencing of ilp7 neurons by hyperpolarization (Kir2.1) but not inhibition of synaptic vesicle release (TnT) impaired nociceptive responses indicated a mechanism independent of direct synaptic neurotransmission (Fig. 4a). Neuropeptide-mediated signaling plays a major role in invertebrate and vertebrate physiology and can strongly modulate the functional state of a circuit[5]. We therefore tested a role for ilp7 peptide in mechano-nociception. Surprisingly, behavioral responses to the 1st stimulus of animals lacking ilp7 peptide ($ilp7^{ko}$) were similarly increased as for optogenetic activation of ilp7 neurons (Supplementary Fig. 5f). However, overall rolling responses were not impaired by the lack of ilp7 peptide suggesting it is not required for mechano-nociceptive behavior. Interestingly, the *Drosophila* NPY homolog sNPF is prominently expressed in DP-ilp7 but not in other ilp7 neurons (Fig. 5a-a", Supplementary Fig. 6a, and ref.[37,38]). We thus carefully examined sNPF localization in DP-ilp7 and sensory da neurons by immunohistochemistry. sNPF was strongly enriched in DP-ilp7 medial and lateral dendrites in apposition to sensory axon terminals including C2da and C4da neurons (Fig. 5a-a"). Additionally, we detected sNPF expression in C4da neurons themselves, both in the axon terminals and soma region (Fig. 5a,b)

This finding prompted us to test a functional role of sNPF in nociceptive behavior. We examined two *sNPF* alleles ($sNPF^{c00448}$ and $sNPF^{MI01807}$) which showed strongly reduced sNPF expression (Supplementary Fig. 6b). Nociceptive rolling after *von Frey* filament stimulation was impaired in *sNPF* homo- or hetero-allelic combinations (Fig. 5c) showing that *sNPF* is necessary for mechano-nociceptive behavior.

We tested if *sNPF* is specifically required in DP-ilp7 or C4da neurons using RNAi-mediated downregulation. sNPF knockdown in ilp7 but not C4da neurons resulted in significantly reduced mechano-nociceptive responses, which was strongly enhanced in heterozygous *sNPF* mutant animals (Fig. 5d, Supplementary Fig. 6c,d). Conversely, expression of transgenic sNPF1 or sNPF2 in ilp7 neurons could significantly rescue mechano-nociceptive behavior (Fig. 5d, Supplementary Fig. 6d). Collectively, these data suggest that *sNPF* function in DP-ilp7 is required for mechano-nociceptive behavior.

sNPF receptor function in mechanosensory da neurons is necessary for nociceptive behavior

The results above implied that DP-ilp7 derived sNPF plays a crucial role in nociceptive behavior. Therefore, we examined sNPF receptor (sNPF-R) expression to identify responsive neuronal subsets. A GFP enhancer trap inserted in the *sNPF-R* locus showed widespread neuronal expression in the VNC ($sNPF\text{-}R^{Mi08722}$). Interestingly, close examination revealed sNPF-R expression was associated with Fas3-labeled axon terminals of C2da, C3da and C4da neurons (Fig. 5e,e'). We then tested the functional requirement of *sNPF-R* for nociceptive behavior in these sensory subsets using RNAi-mediated knockdown or expressing a dominant-negative variant ($sNPF\text{-}R^{DN}$)[39]. Both perturbations in either C2/3da or C4da neurons resulted in strongly impaired mechano-nociceptive responses (Fig. 5f). Interestingly, innocuous touch responses were not affected by the loss of *sNPF-R* function in either C2/3da or C4da neurons showing that sNPF signaling plays a specific role in nociceptive behavior (Supplementary Fig. 6e). We also assayed a potential function of *sNPF-R* in basin neurons, which integrate inputs from chordotonal and C4da neurons to enhance nociceptive rolling[24], but did not detect significant differences in mechano-nociceptive behavior (Supplementary Fig. 6f). These findings show that sensory C2/3da and C4da neurons functionally rely on sNPF signaling to mediate mechano-nociceptive but not innocuous touch responses.

C4da neuron mediated thermo-nociceptive behavior is independent of mechanosensitive circuit components and sensory sNPF signaling

We extended our analysis to thermo-nociception to test if the function of innocuous touch and 2nd order neurons in nociceptive behavior is modality specific. Local exposure to temperatures above 40 °C has been shown to trigger C4da neuron dependent larval rolling[14,16]. We tested larval rolling latencies using a temperature-controlled hot probe for local thermo-nociceptive stimulation. Silencing synaptic output of C4da neurons using TnT strongly increased the response latency compared to controls (Fig. 6a). However, although TnT mediated silencing of C2/3da or A08n neurons strongly impaired mechano-nociceptive behavior, it did not affect thermo-nociceptive responses (Fig. 6b–d). Similarly, neither Kir2.1 nor TnT-mediated inactivation of ilp7 neurons affected this behavior (Fig. 6D, Supplementary Fig. 7A). Although *sNPF* mutant larvae showed mildly increased response latencies (Fig. 6e), C4da neuron specific sNPF-R inactivation by RNAi or dominant negative approaches also did not yield thermo-nociceptive defects (Fig. 6f, Supplementary Fig. 7b). This suggests that sNPF signaling might be important for thermo-nociception in other neuronal subsets.

Collectively, these results show innocuous touch, DP-ilp7, A08n neurons and sensory sNPF signaling are not required for thermo-nociception suggesting a modality specific function.

DP-ilp7 dependent sNPF signaling facilitates C4da neuron synaptic output

To get better insight into *sNPF* function in mechano-nociception, we next tested whether ilp7 neuron activity and sNPF affect presynaptic function of C4da neurons and their output to A08n neurons (Supplementary Fig. 7c,c'). We monitored presynaptic calcium responses in C4da neuron axon terminals and could detect local calcium transients after mechanical stimulation of the corresponding body wall segment (Fig. 7a,a'). However, Kir2.1-mediated ilp7 neuron inhibition significantly reduced presynaptic calcium responses, suggesting that DP-ilp7 neurons provide facilitating feedback to C4da neurons.

We next tested if C4da neuron responses require DP-ilp7 neuron derived sNPF. *sNPF* mutants showed strongly impaired presynaptic calcium responses in C4da neurons after *von Frey* filament stimulation (Fig. 7b,b'). These defects could be rescued by sNPF1 expression in ilp7 neurons, suggesting a paracrine function of sNPF on C4da neuron activity.

Likewise, we tested the requirement of mechano-nociceptive circuit components in regulating A08n neuron responses. Ilp7 neuron inhibition strongly reduced calcium responses of A08n neurons (Fig. 7c,c', Supplementary Fig. 7d,d'). Notable, such reduction was comparable to that induced by inhibition of C4da or C2/3da neurons, suggesting that all identified mechano-sensory circuit components are required for maximum activation of A08n neurons.

To test if sNPF signaling might be the main driving force, we downregulated or inhibited *sNPF-R* function in sensory neurons and measured A08n calcium responses after mechano-nociceptive stimulation. $sNPF\text{-}R^{RNAi}$ or $sNPF\text{-}R^{DN}$ overexpression both resulted in strongly reduced A08n responses (Fig. 7d–e). Interestingly, blocking *sNPF-R* function specifically in C2/C3da or C4da neurons was sufficient to reduce A08n calcium responses. These results show that sNPF-R function in C2/3da and C4da neurons is individually required for full A08n neuron activation after mechano-nociceptive stimulation.

Together, these findings support the idea that mechanosensory activation of DP-ilp7 neurons and their sNPF release to C2da, C3da and C4da neurons is required for facilitation of C4da neuron synaptic output onto A08n neurons.

Discussion

Core and integrating auxiliary nociceptive circuit components are required for escape behavior

Here we identified and characterized a novel and modality-specific node of the nociceptive network required for mechanically induced escape behavior. We demonstrate that C4da neurons form functional synaptic contacts with A08n neurons, which have recently been suggested to be involved in nociceptive behavior[23]. We further show that they respond to mechano-nociceptive stimuli (relayed via C4da neurons) and are necessary and sufficient for nociceptive behavior. Anatomically, our results suggest that A08n neurons are core relay

neurons as they receive input from all C4da neurons and thus potentially convey nociceptive information from anywhere on the body wall.

Moreover, we show that robust escape responses to mechano-nociceptive stimuli require the activity of C2da and C3da sensory neurons, which normally respond to innocuous touch. Intriguingly, we found that neuropeptide-producing DP-ilp7 neurons integrate mechano-sensory input from C2/C3/C4da neurons to facilitate nociceptive escape behavior. DP-ilp7 neurons receive C4da neuron input along the entire VNC (even though such input alone was not sufficient to elicit physiological responses) and can respond to input from touch-responsive C2da neuron as well as coincident activation of C3da and C4da neuron. Thus, innocuous and nociceptive mechanical cues can be integrated – at least in part – by converging onto DP-ilp7 neurons.

Previous results have suggested that C2da and C3da but not C1da neurons respond to mechanical stimulation[12]; further, C3da neuron activity and the mechanosensitive channel NompC are required for innocuous touch[12,13]. In our study, we have found that, curiously, C2da neurons are required in mechano-nociceptive behavior but not innocuous touch responses and that their activation induces C-shape bending and slow rolling which depends partly on ilp7 neuron function. Thus C2da neurons mediate aspects of nociceptive behaviors.

In vertebrates, nociceptive and innocuous touch inputs converge both mono- and polysynaptically within the dorsal horn[1,2,40]. Interestingly, VGLUT3 is specifically expressed in C-low threshold mechanoreceptors and required for injury-induced hypersensitivity to mechanical stimuli, suggesting that vertebrate innocuous touch receptors participate in nociception as well[41]. Consistently, alleviation of mechanically-induced pain require low-threshold mechanoreceptor function in mice[42]. It should be interesting to investigate the mechanism of innocuous and nociceptive touch integration at the network level in higher organisms in more detail.

Multisensory integration of mechanosensory stimuli facilitates modality specific nociceptive behavior

Similarly to most vertebrate nociceptors[1], C4da are multimodal neurons detecting nociceptive mechanical, thermal and aversive light stimuli. Both thermo- and mechano-nociceptive stimulation elicit C4da neuron-dependent rolling and escape responses[14,22], while short-wavelength light triggers an avoidance response[21,43]. How activation of C4da neurons (by different stimuli) produces distinct or seemingly identical nociceptive behaviors is not fully understood. A recent study showed that light and thermal stimulation evoke low-frequency firing trains vs. rapid bursting of C4da neurons, respectively,[44] suggesting that modality-specific physiological responses might be one mechanism. Our data adds another differentiating mechanism: mechano-nociceptive behavior relies on recruitment of discrete network components of the nociceptive network (innocuous touch and DP-ilp7 neurons), which are not required for thermal responses (Supplementary Fig. 7e). Interestingly, TrpA1-expressing neurons in the larval CNS respond to steep temperature gradients and can induce nociceptive rolling[45]. These cells might be connected to C4da neurons suggesting another modality specific subset of the circuit encodes thermo-nociception.

Our findings that inactivation of C2da, C3da or DP-ilp7 neurons virtually completely blocked mechano- but not thermo-nociceptive behavior suggests that the integration of mechanosensory neurons is critical for modality specific escape behavior. While non-nociceptive stimuli alone are not sufficient to trigger nociceptive responses, vibrational stimulation of chordotonal neurons has been shown to enhance C4da-mediated escape behavior[24]. Both sensory pathways are integrated at the 2nd-order level by local basin neurons and further converging on command-like neurons (termed goro) at the 4th level. Similarly, DP-ilp7 neurons provide a neural substrate for innocuous and nociceptive touch integration. Integration of multiple mechanical modalities at multiple levels might protect against predators like the parasitoid wasp *L. boulardi*, which provide multisensory cues (wing beat, innocuous and nociceptive touch) that are very potent in eliciting larval nocifensive responses[22].

sNPF signaling facilitates C4da neuron output and nociceptive behavior

While many components of the nociceptive network in *Drosophila* larvae have been described[24], a role of neuromodulation has not been extensively investigated. We showed that DP-ilp7 neuron activation was sufficient to facilitate mechano-nociceptive behavior. Curiously, sNPF, but not ilp7 peptide expressed in DP-ilp7 neurons plays a critical role in mechano-nociception. sNPF is dendritically localized in DP-ilp7 neurons in direct apposition to sensory nerve terminals. The corresponding sNPF-R is expressed in C2da, C3da and C4da neurons suggesting that sNPF provides an activity dependent regulatory feedback signal within this circuit. Both, reducing functions of sNPF in DP-ilp7 or sNPF-R in sensory C2-4da neurons impaired mechano-nociceptive behavior. Interestingly, sNPF is also localized to C4da neuron axon terminals and its knockdown there leads to thermo-nociceptive hypersensitivity[46]. This raises the possibility that sNPF has distinct functions in nociception depending on when and where it is released.

Drosophila sNPF is involved in feeding[39,47] and sleep[48] behavior. Interestingly, food search behavior in starved animals relies on sNPF dependent presynaptic facilitation in olfactory receptor neurons[49]. Here, we propose that DP-ilp7 neuron activation by sensory neurons results in local sNPF release and feedback facilitation of sensory neuron output via sNPF-R signaling (Supplementary Fig. 7e,f). Our data show that DP-ilp7 activity and sNPF are necessary for full C4da and A08n neuron activation after mechano-nociceptive stimulation suggesting activity-dependent sNPF release is critical for facilitating nociceptive output. Consistently, we found that *sNPF-R* function in C4da neuron was necessary for A08n neuron activation suggesting that sNPF signaling regulates synaptic output. Surprisingly, sNPF-R was functionally and behaviorally required not only in C4da, but also in C2/3da neurons, although they are not directly connected to A08n neurons. It is possible that C2/3da neuron output on DP-ilp7 neurons might be reduced upon sNPF-R inactivation, which in turn reduces sNPF release and C4da neuron output. Alternatively, C2/3da neuron output to additional network components might indirectly regulate A08n activation.

Taken together, we uncovered a mechanism that encodes modality-specific nociceptive behavior through recruitment of specific network components, multisensory integration and neuromodulatory feedback signaling. Interestingly, the closest mammalian homolog of

sNPF-R, NPY receptor 2, is expressed in mechano-nociceptive A-fibers, which mediate paw withdrawal in mice[42]. Moreover, NPY is highly expressed in the dorsal spinal cord and can act to alleviate chronic pain[50]. Thus modality-specific network regulation by NPY and other neuropeptides may have an evolutionarily conserved role in regulating network function under both physiological and pathological conditions[5,6].

Online Methods

Drosophila melanogaster stocks

All stocks were maintained at 25°C and 70% rel. humidity with a 12h light/dark cycle on standard fly food unless noted otherwise. All transgenic lines were maintained in a *white* mutant (w^-) background. C4da neuron specific lines *ppk-Gal4*[51] and *27H06-Gal4/LexA*[23], pan-da neuron line *21-7-Gal4*[52], *2-21-Gal4*[53], *nompC-Gal4*[54], *C1003.3-Gal4*[55], *UAS/LexOP-CsChrimson*[32], *82E12-Gal4/LexA*[23], *UAS/LexOP-GCamP6m*[56], *ppk-Gal80, ilp7-Gal4/LexA*[57], *ppk-CD4-tdTomato, UAS-CD4-tdGFP*[58], *UAS-spGFP1-10-CD4-CFP*[59], *UAS-brp-short-mCherry*[60], *LexAop-brp-short-mCherry*[61], *UAS-Dα7-GFP*[62]. *trpA1-QF, QUAS-rab3-GFP*[63], *tubulin>FRT>Gal80>FRT>*[64], *UAS-Kir2.1*[65], *LexAop-Kir2.1* (this study), *sNPF*^{c00448}, *UAS-sNPF-R-DN, UAS-sNPF-RNAi, UAS-sNPF1, UAS-sNPF2, UAS-sNPF-R-RNAi*[47,66,67] (RNAi#1), *ilp7*^{ko} (*ilp7*^{11})[68]. All other stocks were obtained from the Bloomington, Kyoto, and VDRC stock centers.

Generation of 6.14.3-Gal4, A08n-split-Gal4, 82E12-Gal4^{2nd},UAS-FRT-spGFP1-10-CD4-3×flag6×His-FRT-spGFP11-CD4-tdTomato and DP-ilp7-LexA transgenes

We used the InSITE system Gal4 starter line to generate new Gal4 insertions[28]. Newly generated Gal4 lines were mapped and tested for expression using *UAS-CD4-tdGFP, ppk-CD4-Tomato*. Line *6.14-Gal4* (inserted on a TM6b,Tb balancer chromosome) had a promising expression pattern and was mapped to an insertion within the *rab11* gene using Splinkerette PCR[69]. Defined enhancer fragments flanking the original insertion site were cloned into a Gateway TOPO vector (Life Technologies) and subsequently into the pBPGuw vector[70]. New transgenic lines were generated with phiC31 mediated transgenesis[71] in the attP2 locus (BestGene). A 1.3kb enhancer fragment downstream of the original 6.14 insertion within the *rab11* gene (*6.14.3* primers sequences: TGCTACTACGCCATAAAT and CTGCAAAGGATTAGAGGGAA) showed expression in a small subset of 10–12 CNS neurons including A08n neurons.

We used an intersectional split-Gal4 approach[72] to generate A08n split-Gal4 transgenes. *6.14.3* and *82E12*[23] enhancer fragments were cloned into pBP-ZpGAL4-DBD-Uw (Addgene, #26233) and pBP-p65-ADZp-Uw (Addgene, #26234)[73] to generate Gal4 DNA binding domain (*6.14.3-DBD*) and activation domain (*82E12-AD*) constructs, respectively. Transgenic lines were generated in the attP40 (*82E12-AD*) and attP2 (*6.14.3-DBD*) locus (BestGene) and combined to achieve defined expression in A08n neurons.

A 2nd chromosome insertion of *82E12-Gal4 (82E12-Gal4^{2nd})* was generated by P-element mobilization using transgenic Δ2,3 Transposase and screening for new insertions on the 2nd chromosome.

To generate a CD4 Flip-out cassette, we introduced a 5' FRT site and 3' poly-adenylation sequences (from Histone 2A1) into MultiSite Gateway pENTRY vectors (ThermoFisher). We then subcloned split-GFP carrying CD4-CFP and CD4-tdTomato cDNAs into complementary pENTRY vectors (pENTRY-FRT-CD4sp1-10-CFP-3×polyA and pENTRY-FRT-CD4sp11-tdTomato-polyA, respectively). We then combined both pENTRY plasmids into a pDEST vector (containing 5×UAS sites1 using a 3-way Gateway reaction. Transgenic lines were generated in the attP2 locus (BestGene).

To generate a DP-ilp7 specific line (*DP-ilp7-LexA*), 1099 bp of a DNA element at the 5' end of the ilp7 gene (starting from −1131 until −33, ATG for ILP7 starts at position 0) was cloned by PCR amplification into the pBPLexA::p65Uw vector[73]. Transgenic lines were generated in the attP2 locus (BestGene).

Immunohistochemistry and confocal microscopy

Larval brain preparation and staining was essentially performed as described[51]. Briefly, larval brains were dissected in PBS and fixed with 4% Formaldehyde/PBS for 15min, washed with PBS and mounted on poly-L-Lysine (Sigma) coated cover slips in SlowFade Gold (Life Technologies). For most samples, native fluorescence was sufficiently bright and was subsequently visualized by confocal microscopy (Zeiss LSM700). Confocal z-stacks were processed in Fiji (ImageJ, NIH, Bethesda) and/or Imaris (BitPlane).

For activity dependent GFP-reconstitution across synaptic partners (Syb-GRASP)[29], we examined native GFP fluorescence after fixation together with an anti-GFP antibody recognizing the spGFP1-10 fragment (rabbit anti-GFP, 1:500, #A-11122, ThermoFisher).

Drosophila mouse anti-Fas3 was used as a sensory axon marker (7G10[74], 1:100, DSHB, Iowa), rat anti-N-Cadherin (DN-Ex#8[75], 1:100, DSHB, Iowa) and mouse anti-Brp (nc82[76], 1:100, DSHB, Iowa) antibodies were used as neuropil markers. For sNPF immunostaining, a rabbit anti-sNPF antibody recognizing the sNPF pro-protein was used[38,77] (1:4000, kind gift of J. Veenstra).

Secondary donkey antibodies conjugated to DyLight dyes were used at 1:300 dilution (Jackson ImmunoResearch). Confocal imaging was performed as described above. All experiments have been performed at least three times examining multiple animals with consistent results (5–10 animals/experiment)

Immuno-transmission electron microscopy (TEM)

We used a protocol previously described for TEM and DAB-specific labeling[58,78] with adaptations to the use of antibody labeling in larval brains. In order to specifically visualize C4da neuron presynaptic vesicles and A08n neuronal processes, we expressed GFP-tagged rab3 (*trpA1-QF, QUAS-rab3-GFP*) and a CD4 membrane-tagged GFP (*6.14.3-Gal4, UAS-CD4-tdGFP*), respectively. For investigating sensory neuron and DP-ilp7 synaptic contact we used mCherry-tagged Brp-short (*21-7-Gal4, UAS-Brp-short-mCherry*) and CD4-tdTomato (*ilp7-LexA, LexAOP-CD4tdTomato*) as a membrane label. 3rd instar larval brains were dissected in cold 0.1M Sorensen's Phosphate Buffer (SPB, Electron Microscopy Sciences) and fixed with Periodate-lysine-paraformaldehyde (PLP, Electron Microscopy

Sciences) fixative for 20 min, followed by fixation in 0.01% glutaraldehyde in SPB for 30 min at RT. Free aldehyde was quenched with 1mM Glycine in SPB for 10 min. To allow antibody penetration through the blood brain barrier, it was necessary to carefully puncture the brain surface with an electrolytically sharpened tungsten needle. Subsequently, 0.3% H_2O_2 was applied for 30 min to block endogenous peroxidase activity. After washing and blocking buffer containing SPB and 0.25% Saponin (Sigma-Aldrich), the specimens were stained with a rabbit anti-GFP antibody (C4da-A08n, 1:500, #A-11122, ThermoFisher) or with a rabbit anti-DsRed antibody (sensory-ilp7, 1:500, #632496, ClonTech)[51] in blocking solution, followed by the VectaStain ABC kit procedure with a biotinylated anti-rabbit secondary antibody and HRP (Vector Laboratories). Samples were then incubated in SPB containing 0.5 mg/ml DAB and 0.003% H_2O_2 to visualize HRP activity. Stained specimens were post fixed in 2% GA in SPB for 1h for and then treated with 1% OsO_4 for 1 h on ice. After dehydration ethanol series, the specimens were embedded in epon (Roth). 0.5 μm semi-thin cross-sections of the VNC were cut and examined under the light microscope to find DAB stained areas with labeled neuronal structures. Ultrathin sections (60 nm) were examined on an EM902 (Zeiss, Germany). Serial sections from multiple animals (n>3) were examined and pictures were taken with a MegaViewIII digital camera (A. Tröndle, Moorenweis, Germany).

Blinding and randomization

All behavioral assays were performed in a blinded fashion. The order of tested genotypes was randomized. *Post-hoc* video analyses of optogenetic and thermo-nociception behavior was also randomized based on arbitrary numbering of videos. Scoring of behavioral responses was performed blindly.

Optogenetic activation assays

Optogenetic assays with staged 3rd instar larvae (96h AEL) were essentially performed as described[79], except that CsChrimson mediated activation was used. Embryos were collected on grape juice agar plates and supplied with fresh yeast paste containing 5mM all-trans-retinal and kept at 25 °C in the dark. Staged and density controlled 3rd instar larvae (96h±3h AEL) were then collected under low red light illumination and 15–20 larvae/experiment were assayed on a 10 cm 2% agar dish containing 1ml of water. Larvae were kept in a dark box illuminated only by a custom made infrared light frame and videotaped. CsChrimson activation was performed by illumination with a 625 nm light source (LED backlight Phlox RGB-BL-S-Q-1R, 2000 cd/m^2, Phlox Corp.) for 5 s at 0.2 mW/mm^2. Videos were analyzed in a blinded fashion offline and scored for nociceptive rolling during the 5 s activation period. Each genotype was tested multiple times on different days and data from all trials was combined. Statistical significance was assessed by the chi^2 test (n>100).

Mechano- and thermo-nociception assays

Experiments were performed with staged 3rd instar larvae as described for mechano[22]- and thermo-nociception assays[14,16]. Animals were staged for 6h and allowed to develop for 4 days (96h±3h AEL).

For mechano-nociception, forward locomoting larvae were stimulated on mid-abdominal segments (a3–5) with a 45 mN *von Frey* filament twice within 2s. Each behavioral response was scored as non-nociceptive (no response, stop, stop and turn) or nociceptive (bending, rolling). Rolling and bending behavior was classified as nociceptive due to their absence in *TrpA1* mutant animals. Stopping, turning or no response were scored as non-nociceptive behaviors. For simultaneous CsChrimson activation, all-*trans*-Retinal fed larvae35 were stimulated with simultaneous acute exposure to 625 nm light using a Xenon light source coupled stereoscope (10 mW/mm^2, Olympus). Each genotype was tested multiple times on different days and data from all trials was combined. Statistical significance was calculated using the chi^2 test.

For thermo-nociception using a local hot probe, a custom-built thermo-couple device was used to keep the applied temperature constantly at 46 °C. Stage and density controlled 3rd instar larvae (96h±3h AEL) were used and all experiments were performed in a blinded fashion. Forward locomoting larvae were touched with the hot probe on mid-abdominal segments (a4–6) until the execution of nociceptive rolling (up to 10 s). Animals were videotaped and rolling latencies analyzed in a blinded fashion using ImageJ (NIH, Bethesda). Each genotype was tested multiple times on different days and data from all trials was combined. Statistical significance was calculated using Kruskal-Wallis ANOVA and pairwise comparison with Dunn's *post hoc* test.

Gentle touch assays

Gentle touch assays were performed and scored according to Kernan *et al.*[80] in a blinded fashion. Staged and density controlled 3rd instar larvae (96h±3h AEL) were touched on the 2^{nd} thoracic segment with an eyelash for four times. Each reaction was scored and summed up as a touch score. Each genotype was tested multiple times on different days and data from all trials was combined. Touch scores were represented as box-plots with whiskers, with the centerline representing median values, upper and lower edges of the boxes representing the 25^{th} and 75^{th} percentiles of the sample data, respectively. The short line within the box represents the mean of the data. Upper and lower whiskers represent the 5^{th} and 95th percentile of the sample data, respectively. Statistical significance was calculated using the nonparametric Mann-Whitney test.

Larval locomotion analysis

Larval locomotion analysis was performed using a FTIR (frustrated total internal reflection) based tracking system (FIM, University of Münster)[81]. Five freely moving larvae/trial were video-captured for 1 min and average locomotion speed was analyzed using FIMtracking software (FIM, University of Münster). Each genotype was tested multiple times on different days and data from all trials was combined. Average velocities were represented as box-plots with whiskers, with the centerline representing median values, upper and lower edges of the boxes representing the 25^{th} and 75^{th} percentiles of the sample data, respectively. The short line within the box represents the mean of the data. Upper and lower whiskers represent the 5^{th} and 95th percentile of the sample data, respectively. Statistical significance was calculated using the nonparametric Mann-Whitney test.

GCaMP6m Calcium imaging

Staged 3rd instar larvae (96h AEL±3h AEL) were pinned on a Sylgard (Dow Corning) plate and partially dissected in physiological saline[21] to expose the VNC. A08n or DP-ilp7 neuron somata or C4da neuron axon terminals expressing GCaMP6m were live imaged by confocal microscopy with a 40× water objective (Olympus FV1000MP). Activation of sensory neurons was achieved either by class specific expression of CsChrimson (625 nm/5 s, 0.2 mW/mm^2) or providing a mechano-nociceptive cue using a micromanipulator mounted *von Frey* filament (45 mN) and stimulation of mid-abdominal segments (a3–5). Baseline (F_0) and relative maximum intensity change (F_{max}) of GCaMP6m fluorescence was analyzed. F_{max}/F_0 values were represented as box-plots with whiskers, with the centerline representing median values, upper and lower edges of the boxes representing the 25th and 75th percentiles of the sample data, respectively. The short line within the box represents the mean of the data. Upper and lower whiskers represent the 5th and 95th percentile of the sample data, respectively. Statistical significance was analyzed using Mann-Whitney U-test with Bonferroni correction for multiple comparisons.

Statistics

No statistical methods were used to predetermine sample sizes, but sample sizes were chosen to be similar to those reported in previous publications[15,16,22,49,79,80]. Normal data distribution was tested using a Shapiro-Wilkinson test. If normality was given, two-tailed unpaired Student's *t*-test and chi-squared tests were used to compare two groups. If normality was not given, a non-parametric Mann-Whitney U-test was used. For multiple comparisons of categorized thermo-nociception data, a Kruskal-Wallis ANOVA with Dunn's *post-hoc* comparison was performed. Statistical differences were considered significant for $p<0.05$ (*:$p<0.05$, **:$p<0.01$, ***:$p<0.001$). Statistical testing was performed using Origin Pro (OriginLab Corp.), SigmaPlot (Systat Software Inc.) and Excel (Microsoft Corp.).

A Supplementary Methods Checklist is available.

The data that support the findings of this study are available from the corresponding author upon reasonable request.

Supplementary Material

Refer to Web version on PubMed Central for supplementary material.

Acknowledgments

Stocks obtained from the Bloomington (NIH P40OD018537), VDRC, and Kyoto *Drosophila* Stock Centers were used in this study. Antibodies were obtained from the Developmental Studies Hybridoma Bank (created by the NICHD/NIH, maintained at The University of Iowa). We thank S. Sigrist for *UAS-Brp-short-mCherry* and *UAS-Da7-GFP*, G. Tavosanis for the *LexOP-brp-short-mCherry*, K. Yu for *sNPF* and *sNPF-R* lines, J. Veenstra for sNPF antibodies. D. Pauls for helpful discussion and reagents, T. Oertner, S. Wiegert, D. Pauls, J. Parrish, S. Zhu, C. Han, K. Duncan and F. Calderon for critical reading of the manuscript, W. Grueber, A. Cardona and M. Zlatic for communicating results prior to publication. This work was supported by National Institutes of Health (NIH) grant R01GM100027 (to A.G. and C.H.Y.), the Landesförschungsförderung LFF-FV27 (to. P.S.) and the Deutsche Forschungsgemeinschaft priority program SPP1926, project SO1337/2-1 (to P.S.).

References

1. Dubin AE, Patapoutian A. Nociceptors: The sensors of the pain pathway. J. Clin. Invest. 2010; 120:3760–3772. [PubMed: 21041958]
2. Basbaum AI, Bautista DM, Scherrer G, Julius D. Cellular and molecular mechanisms of pain. Cell. 2010; 139:267–284.
3. Lumpkin EA, Caterina MJ. Mechanisms of sensory transduction in the skin. Nature. 2007; 445:858–65. [PubMed: 17314972]
4. Taghert PH, Nitabach MN. Peptide neuromodulation in invertebrate model systems. Neuron. 2012; 76:82–97. [PubMed: 23040808]
5. Marder E. Neuromodulation of neuronal circuits: back to the future. Neuron. 2012; 76:1–11. [PubMed: 23040802]
6. Bargmann CI. Beyond the connectome: How neuromodulators shape neural circuits. BioEssays. 2012; 34:458–465. [PubMed: 22396302]
7. Nässel DR, Winther AME. Drosophila neuropeptides in regulation of physiology and behavior. Prog. Neurobiol. 2010; 92:42–104. [PubMed: 20447440]
8. Im SH, et al. Tachykinin acts upstream of autocrine Hedgehog signaling during nociceptive sensitization in Drosophila. Elife. 2015; 4:1689–1699.
9. Ghysen A, Dambly-Chaudière C, Aceves E, Jan L-Y, Jan Y-N. Sensory neurons and peripheral pathways in Drosophila embryos. Roux's Arch. Dev. Biol. 1986; 195:281–289. [PubMed: 28306052]
10. Bodmer R, Jan YN. Morphological differentiation of the embryonic peripheral neurons in Drosophila. Roux's Arch. Dev. Biol. 1987; 196:69–77. [PubMed: 28305460]
11. Grueber WB, Jan LY, Jan YN. Tiling of the Drosophila epidermis by multidendritic sensory neurons. Development. 2002; 129:2867–2878. [PubMed: 12050135]
12. Tsubouchi A, Caldwell JC, Tracey WD. Dendritic filopodia, Ripped Pocket, NOMPC, and NMDARs contribute to the sense of touch in Drosophila larvae. Curr. Biol. 2012; 22:2124–34. [PubMed: 23103192]
13. Yan Z, et al. Drosophila NOMPC is a mechanotransduction channel subunit for gentle-touch sensation. Nature. 2013; 493:221–5. [PubMed: 23222543]
14. Tracey WD, Wilson RI, Laurent G, Benzer S. painless, a Drosophila gene essential for nociception. Cell. 2003; 113:261–73. [PubMed: 12705873]
15. Zhong L, Hwang RY, Tracey WD. Pickpocket is a DEG/ENaC protein required for mechanical nociception in Drosophila larvae. Curr Biol. 2010; 20:429–434. [PubMed: 20171104]
16. Zhong L, et al. Thermosensory and nonthermosensory isoforms of Drosophila melanogaster TRPA1 reveal heat-sensor domains of a thermoTRP Channel. Cell Rep. 2012; 1:43–55. [PubMed: 22347718]
17. Gorczyca, Da, et al. Identification of Ppk26, a DEG/ENaC Channel Functioning with Ppk1 in a Mutually Dependent Manner to Guide Locomotion Behavior in Drosophila. Cell Rep. 2014; 9:1446–58. [PubMed: 25456135]
18. Guo Y, Wang Y, Wang Q, Wang Z. The Role of PPK26 in Drosophila Larval Mechanical Nociception. Cell Rep. 2014; 9:1183–1190. [PubMed: 25457610]
19. Kim SE, Coste B, Chadha A, Cook B, Patapoutian A. The role of Drosophila Piezo in mechanical nociception. Nature. 2012; 483:209–12. [PubMed: 22343891]
20. Neely GG, et al. A genome-wide Drosophila screen for heat nociception identifies α2δ3 as an evolutionarily conserved pain gene. Cell. 2010; 143:628–38. [PubMed: 21074052]
21. Xiang Y, et al. Light-avoidance-mediating photoreceptors tile the Drosophila larval body wall. Nature. 2010; 468:921–6. [PubMed: 21068723]
22. Hwang RY, et al. Nociceptive neurons protect Drosophila larvae from parasitoid wasps. Curr Biol. 2007; 17:2105–2116. [PubMed: 18060782]
23. Vogelstein JT, et al. Discovery of brainwide neural-behavioral maps via multiscale unsupervised structure learning. Science. 2014; 344:386–92. [PubMed: 24674869]

24. Ohyama T, et al. A multilevel multimodal circuit enhances action selection in Drosophila. Nature. 2015; 520:633–639. [PubMed: 25896325]
25. Fetsch CR, DeAngelis GC, Angelaki DE. Bridging the gap between theories of sensory cue integration and the physiology of multisensory neurons. Nat. Rev. Neurosci. 2013; 14:429–442. [PubMed: 23686172]
26. van Atteveldt N, Murray MM, Thut G, Schroeder CE. Multisensory Integration: Flexible Use of General Operations. Neuron. 2014; 81:1240–1253. [PubMed: 24656248]
27. Stein BE, Stanford TR, Rowland Ba. Development of multisensory integration from the perspective of the individual neuron. Nat. Rev. Neurosci. 2014; 15:520–535. [PubMed: 25158358]
28. Gohl DM, et al. A versatile in vivo system for directed dissection of gene expression patterns. Nat Methods. 2011; 8:231–237. [PubMed: 21473015]
29. Frank DD, Jouandet GC, Kearney PJ, Macpherson LJ, Gallio M. Temperature representation in the Drosophila brain. Nature. 2015; 2:358–361.
30. Miguel-Aliaga I, Thor S, Gould AP. Postmitotic specification of Drosophila insulinergic neurons from pioneer neurons. PLoS Biol. 2008; 6:e58. [PubMed: 18336071]
31. Grueber WB, et al. Projections of Drosophila multidendritic neurons in the central nervous system: links with peripheral dendrite morphology. Development. 2007; 134:55–64. [PubMed: 17164414]
32. Klapoetke NC, et al. Independent optical excitation of distinct neural populations. Nat. Methods. 2014; 11:338–46. [PubMed: 24509633]
33. Yang L, et al. Trim9 Regulates Activity-Dependent Fine-Scale Topography in Drosophila. Curr. Biol. 2014:1–7.
34. Zhang W, Yan Z, Li B, Jan LY, Jan YN. Identification of motor neurons and a mechanosensitive sensory neuron in the defecation circuitry of Drosophila larvae. Elife. 2014; 3
35. Robertson JL, Tsubouchi A, Tracey WD. Larval Defense against Attack from Parasitoid Wasps Requires Nociceptive Neurons. PLoS One. 2013; 8:e78704. [PubMed: 24205297]
36. Turner HN, et al. The TRP Channels Pkd2, NompC, and Trpm Act in Cold-Sensing Neurons to Mediate Unique Aversive Behaviors to Noxious Cold in Drosophila. Curr. Biol. 2016; 26:3116–3128. [PubMed: 27818173]
37. Carlsson, Ma, Enell, LE., Nässel, DR. Distribution of short neuropeptide F and its receptor in neuronal circuits related to feeding in larval Drosophila. Cell Tissue Res. 2013; 353:511–23. [PubMed: 23760890]
38. Nässel DR, Enell LE, Santos JG, Wegener C, Johard HAD. A large population of diverse neurons in the Drosophila central nervous system expresses short neuropeptide F, suggesting multiple distributed peptide functions. BMC Neurosci. 2008; 9:90. [PubMed: 18803813]
39. Lee K-S, et al. Drosophila short neuropeptide F signalling regulates growth by ERK-mediated insulin signalling. Nat. Cell Biol. 2008; 10:468–475. [PubMed: 18344986]
40. Abraira V, Ginty D. The sensory neurons of touch. Neuron. 2013; 79:618–639. [PubMed: 23972592]
41. Seal RP, et al. Injury-induced mechanical hypersensitivity requires C-low threshold mechanoreceptors. Nature. 2009; 462:651–5. [PubMed: 19915548]
42. Arcourt A, et al. Touch Receptor-Derived Sensory Information Alleviates Acute Pain Signaling and Fine-Tunes Nociceptive Reflex Coordination. Neuron. 2016; 93:179–193. [PubMed: 27989460]
43. Yamanaka N, et al. Neuroendocrine Control of Drosophila Larval Light Preference. Science. 2013; 341:1113–1116. [PubMed: 24009394]
44. Terada S-I, et al. Neuronal processing of noxious thermal stimuli mediated by dendritic Ca(2+) influx in Drosophila somatosensory neurons. Elife. 2016; 5:e12959. [PubMed: 26880554]
45. Luo J, Shen WL, Montell C. TRPA1 mediates sensation of the rate of temperature change in Drosophila larvae. Nat. Neurosci. 2016; 20:34–41. [PubMed: 27749829]
46. Honjo K, Mauthner SE, Wang Y, Skene JHP, Tracey WD. Nociceptor-Enriched Genes Required for Normal Thermal Nociception. Cell Rep. 2016; 16:295–303. [PubMed: 27346357]
47. Lee KS, You KH, Choo JK, Han YM, Yu K. Drosophila short neuropeptide F regulates food intake and body size. J. Biol. Chem. 2004; 279:50781–50789. [PubMed: 15385546]

48. Shang Y, et al. Short Neuropeptide F Is a Sleep-Promoting Inhibitory Modulator. Neuron. 2013; 80:171–183. [PubMed: 24094110]
49. Root CM, Ko KI, Jafari A, Wang JW. Presynaptic Facilitation by Neuropeptide Signaling Mediates Odor-Driven Food Search. Cell. 2011; 145:133–144. [PubMed: 21458672]
50. Solway B, Bose SC, Corder G, Donahue RR, Taylor BK. Tonic inhibition of chronic pain by neuropeptide Y. Proc. Natl. Acad. Sci. U. S. A. 2011; 108:7224–9. [PubMed: 21482764]
51. Han C, Jan LY, Jan Y-NN. Enhancer-driven membrane markers for analysis of nonautonomous mechanisms reveal neuron-glia interactions in Drosophila. Proc Natl Acad Sci U S A. 2011; 108:9673–9678. [PubMed: 21606367]
52. Song W, Onishi M, Jan LY, Jan YN. Peripheral multidendritic sensory neurons are necessary for rhythmic locomotion behavior in Drosophila larvae. Proc Natl Acad Sci U S A. 2007; 104:5199–5204. [PubMed: 17360325]
53. Parrish JZ, Kim MD, Jan LY, Jan YN. Genome-wide analyses identify transcription factors required for proper morphogenesis of Drosophila sensory neuron dendrites. Genes Dev. 2006; 20:820–35. [PubMed: 16547170]
54. Shearin HK, Dvarishkis AR, Kozeluh CD, Stowers RS. Expansion of the Gateway MultiSite Recombination Cloning Toolkit. PLoS One. 2013; 8:1–14.
55. Hughes CL, Thomas JB. A sensory feedback circuit coordinates muscle activity in Drosophila. Mol. Cell. Neurosci. 2007; 35:383–96. [PubMed: 17498969]
56. Chen T-W, et al. Ultrasensitive fluorescent proteins for imaging neuronal activity. Nature. 2013; 499:295–300. [PubMed: 23868258]
57. Yang CH, Belawat P, Hafen E, Jan LY, Jan YN. Drosophila egg-laying site selection as a system to study simple decision-making processes. Science. 2008; 319:1679–1683. [PubMed: 18356529]
58. Han C, et al. Integrins regulate repulsion-mediated dendritic patterning of drosophila sensory neurons by restricting dendrites in a 2D space. Neuron. 2012; 73:64–78. [PubMed: 22243747]
59. Jiang N, Soba P, Parker E, Kim CC, Parrish JZ. The microRNA bantam regulates a developmental transition in epithelial cells that restricts sensory dendrite growth. Development. 2014:2657–2668. [PubMed: 24924190]
60. Leiss F, et al. Characterization of dendritic spines in the Drosophila central nervous system. Dev. Neurobiol. 2009; 69:221–34. [PubMed: 19160442]
61. Berger-Müller S, et al. Assessing the role of cell-surface molecules in central synaptogenesis in the Drosophila visual system. PLoS One. 2013; 8:e83732. [PubMed: 24386266]
62. Christiansen F, et al. Presynapses in Kenyon cell dendrites in the mushroom body calyx of Drosophila. J. Neurosci. 2011; 31:9696–707. [PubMed: 21715635]
63. Potter CJ, Tasic B, Russler EV, Liang L, Luo L. The Q system: a repressible binary system for transgene expression, lineage tracing, and mosaic analysis. Cell. 2010; 141:536–548. [PubMed: 20434990]
64. Gordon MD, Scott K. Motor control in a Drosophila taste circuit. Neuron. 2009; 61:373–384. [PubMed: 19217375]
65. Baines RA, Uhler JP, Thompson A, Sweeney ST, Bate M. Altered electrical properties in Drosophila neurons developing without synaptic transmission. J. Neurosci. Off. J. Soc. Neurosci. 2001; 21:1523–1531.
66. Hong SH, et al. Minibrain/Dyrk1a regulates food intake through the Sir2-FOXO-sNPF/NPY pathway in Drosophila and mammals. PLoS Genet. 2012; 8:e1002857. [PubMed: 22876196]
67. Lee KS, et al. Processed short neuropeptide F peptides regulate growth through the ERK-insulin pathway in Drosophila melanogaster. FEBS Lett. 2009; 583:2573–2577. [PubMed: 19619547]
68. Grönke S, Clarke D-F, Broughton S, Andrews TD, Partridge L. Molecular evolution and functional characterization of Drosophila insulin-like peptides. PLoS Genet. 2010; 6:e1000857. [PubMed: 20195512]
69. Potter CJ, Luo L. Splinkerette PCR for mapping transposable elements in Drosophila. PLoS One. 2010; 5:e10168. [PubMed: 20405015]

70. Pfeiffer BD, Truman JW, Rubin GM. Using translational enhancers to increase transgene expression in Drosophila. Proc. Natl. Acad. Sci. U. S. A. 2012; 109:6626–31. [PubMed: 22493255]

71. Groth AC, Fish M, Nusse R, Calos MP. Construction of transgenic Drosophila by using the site-specific integrase from phage phiC31. Genetics. 2004; 166:1775–82. [PubMed: 15126397]

72. Luan H, Peabody NC, Vinson CR, White BH. Refined spatial manipulation of neuronal function by combinatorial restriction of transgene expression. Neuron. 2006; 52:425–36. [PubMed: 17088209]

73. Pfeiffer BD, et al. Refinement of tools for targeted gene expression in Drosophila. Genetics. 2010; 186:735–55. [PubMed: 20697123]

74. Patel NH, Snow PM, Goodman CS. Characterization and cloning of fasciclin III: a glycoprotein expressed on a subset of neurons and axon pathways in Drosophila. Cell. 1987; 48:975–88. [PubMed: 3548998]

75. Iwai Y, et al. Axon patterning requires DN-cadherin, a novel neuronal adhesion receptor, in the Drosophila embryonic CNS. Neuron. 1997; 19:77–89. [PubMed: 9247265]

76. Wagh DA, et al. Bruchpilot, a Protein with Homology to ELKS/CAST, Is Required for Structural Integrity and Function of Synaptic Active Zones in Drosophila. Neuron. 2006; 49:833–844. [PubMed: 16543132]

77. Johard HAD, et al. Intrinsic neurons of Drosophila mushroom bodies express short neuropeptide F: Relations to extrinsic neurons expressing different neurotransmitters. J. Comp. Neurol. 2008; 507:1479–1496. [PubMed: 18205208]

78. Lin DM, Fetter RD, Kopczynski C, Grenningloh G, Goodman CS. Genetic analysis of Fasciclin II in drosophila: Defasciculation, refasciculation, and altered fasciculation. Neuron. 1994; 13:1055–1069. [PubMed: 7946345]

79. Honjo K, Hwang RY, Tracey WD. Optogenetic manipulation of neural circuits and behavior in Drosophila larvae. Nat. Protoc. 2012; 7:1470–8. [PubMed: 22790083]

80. Kernan M, Cowan D, Zuker C. Genetic dissection of mechanosensory transduction: Mechanoreception-defective mutations of drosophila. Neuron. 1994; 12:1195–1206. [PubMed: 8011334]

81. Risse B, et al. FIM, a novel FTIR-based imaging method for high throughput locomotion analysis. PLoS One. 2013; 8:e53963. [PubMed: 23349775]

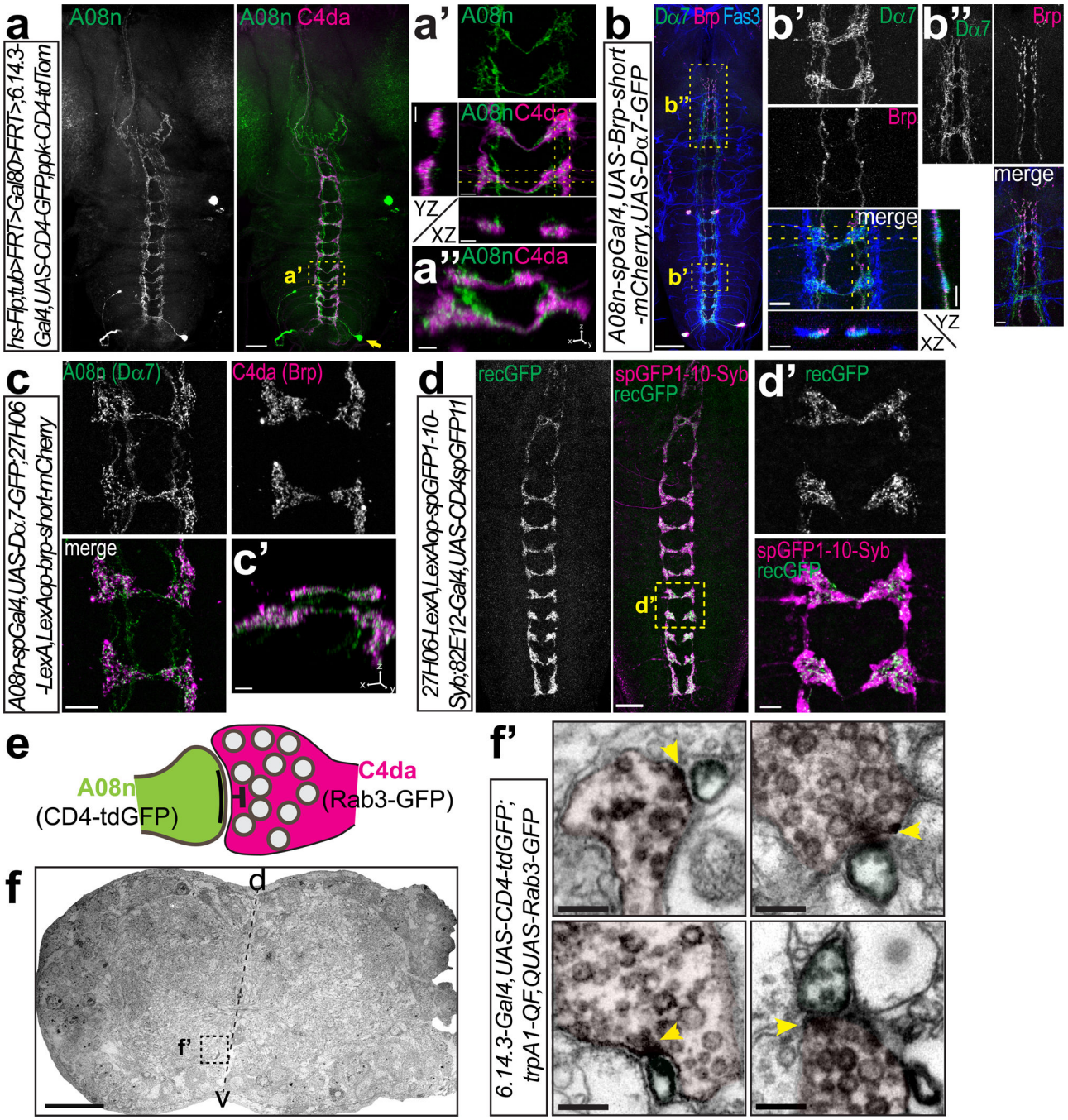

Figure 1. A08n neurons receive synaptic input from C4da neurons

(a) A08n single-cell morphology visualized by Flp-mediated CD4-tdGFP labeling together with C4da neuron axon morphology. Scale bar: 50 μm. (a') Enlarged view of boxed area in (a) and YZ and XZ projections of the indicated sections (dotted lines). (a") 3D-view of (a'). Scale bars: 5 μm. (b) A08n neurons labeled by *A08n-spGal4* expressing presynaptic Brp-short-mCherry and postsynaptic Dα7-GFP markers together with anti-Fas3 antibody labeling (Scale bar: 50 μm). Boxed region shows Dα7-positive postsynaptic sites along anti-Fas3 labeled sensory terminals with maximal projections resliced along the YZ and XZ axis

(indicated by dotted lines) (b'), and Brp-positive A08n axon terminals in the GNG (b"). Scale bars: 10 μm. (c) Expression of Dα7-GFP in A08n neurons and Brp-short-mCherry in C4da neurons shows specific overlap. (c') 3D-view of (c). Scale bars: 10 and 5 μm. (d) Syb-GRASP between C4da and A08n neurons displays GFP reconstitution along the entire VNC. Scale bar: 25 μm. (d') Enlarged view of boxed area in (d). Scale bar: 5 μm. (e) Schematic model of a C4da-A08n synapse visualized by DAB-labeled plasma membrane (CD4-tdGFP in A08n) and presynaptic vesicle markers (Rab3-GFP in C4da). (f) Semi-thin VNC cross-section with specific DAB labeling in the boxed ventromedial region of the neuropil. Scale bar: 25 μm (f') Examples of C4da presynaptic contact (magenta) with A08n neurons (green). T-bar region indicated by yellow arrows. Scale bars: 200 nm.

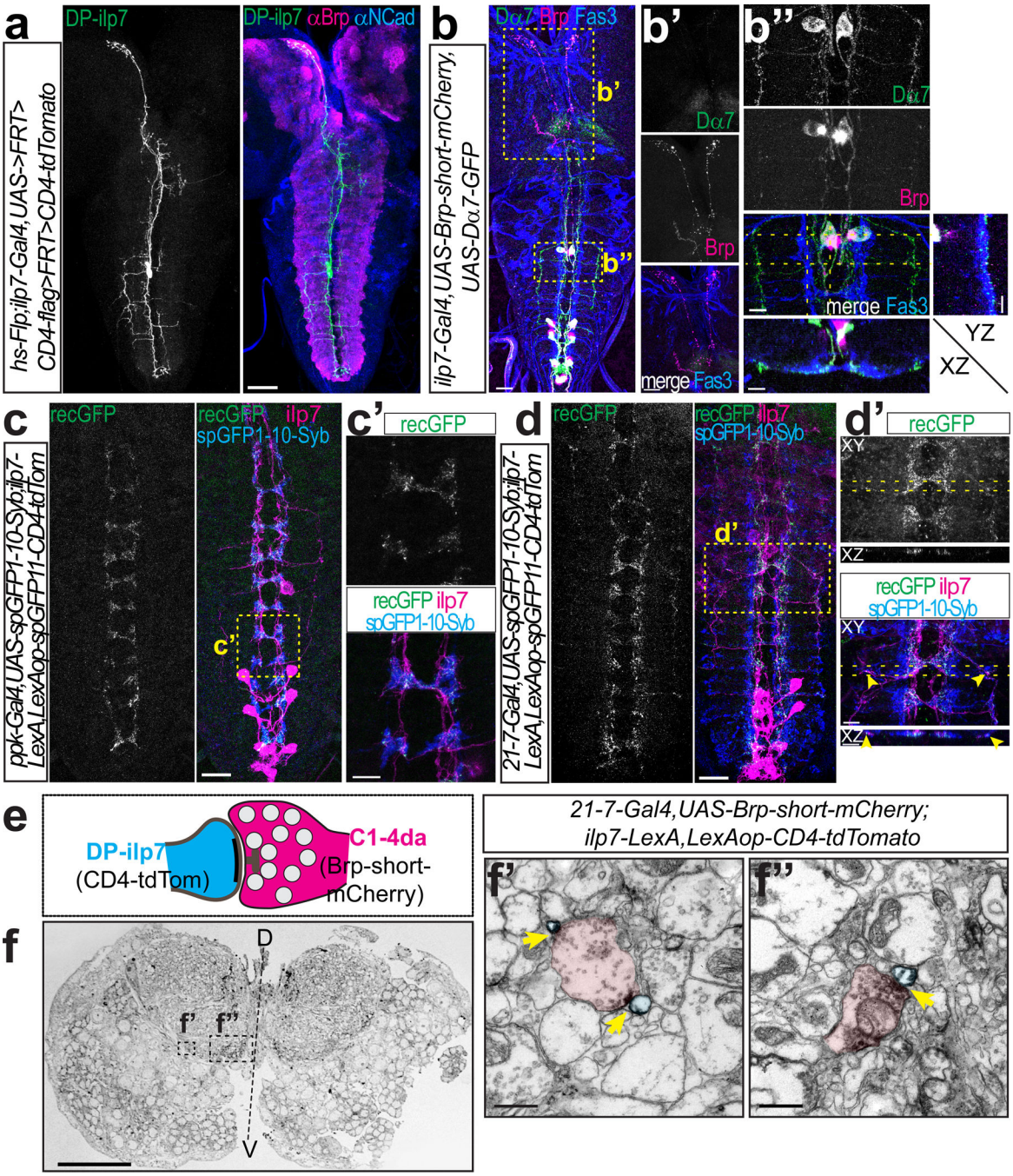

Figure 2. DP-ilp7 neurons are connected to multiple classes of sensory da neurons

(a) DP-ilp7 neuron morphology visualized by Flp-mediated CD4-tdTomato labeling together with neuropil markers (anti-Brp in magenta, anti-N-Cadherin in blue). Scale bar: 50 μm. (b) Ilp7 neurons expressing presynaptic Brp-short-mCherry and postsynaptic Dα7-GFP markers together with anti-Fas3 labeling (Scale bar: 25 μm). Boxed regions show (b') Brp-positive DP-ilp7 axon terminals in the PI region and (b") Dα7-positive postsynaptic sites of DP-ilp7 neurons align with Fas3-labeled sensory terminals (YZ and XZ resliced projections indicated by dotted lines). Scale bars: 10 μm. (c) Syb-GRASP showing native reconstituted

GFP signal (recGFP) between C4da (Syb-GFPsp1-10) and DP-ilp7 neurons (GFPsp11-CD4-tdTomato). Scale bar: 25 μm. (c') Enlarged view of boxed region in (c). Scale bar: 5 μm. (d) Syb-GRASP between sensory da neuron expressed Syb-GFPsp1-10 (anti-GFPsp1-10) and DP-ilp7 neurons (GFPsp11-CD4-tdTomato) shows native reconstituted GFP (recGFP) along ventromedial and -lateral DP-ilp7 projections. Scale bar: 25 μm. (d') Enlarged view of boxed region in (d). Arrowheads indicate lateral synapses of DP-ilp7 with C2da neurons. Scale bars: 5 μm. (e) Schematic of a sensory-DP-ilp7 neuron synapse visualized by DAB-labeled plasma membrane (CD4-tdTomato in ilp7) and sensory da neuron presynaptic active zone markers (Brp-short-mCherry). (f) Semi-thin VNC cross-section with specific DAB-labeling in the ventro-lateral and –medial neuropil. Scale bar: 25 μm. Ultrathin section of (f') ventrolateral presynaptic terminals (C2da) contacting DP-ilp7 neurons and (f") ventromedial contact between da neurons (C4da) and DP-ilp7 neurons. DAB-labeled active zones are indicated by arrows. Scale bars: 1 μm.

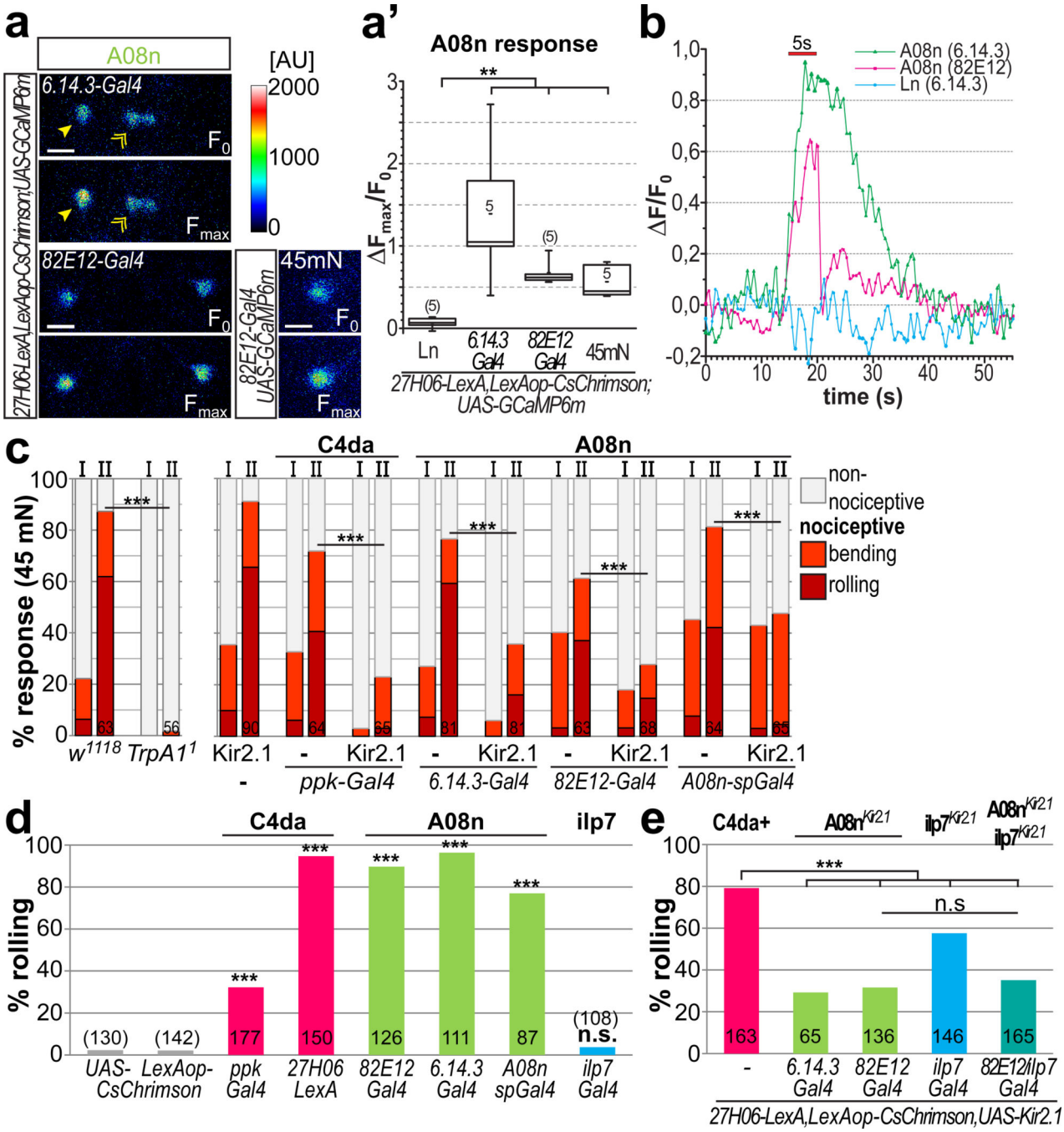

Figure 3. A08n neurons are necessary and sufficient for nociceptive responses downstream of C4da neurons

(a) GCaMP6m expressing A08n (arrowhead) or local interneurons (Ln, labeled by *6.14.3-Gal4*, indicated by double arrow) before (F_0) or after CsChrimson-mediated optogenetic activation of C4da neurons (*6.14.3-Gal4* or *82E12-Gal4*, F_{max} after 5 s 625 nm light pulse, 0.2 mW/mm^2) or mechano-nociceptive stimulation with a 45 mN *von Frey* filament (*82E12-Gal4*). (a') Maximum responses ($\Delta F_{max}/F_0$) were plotted showing that C4da neuron activation or mechano-nociceptive stimulation specifically activate A08n but not Ln neurons (n=5 each, $p<0.01$, Mann-Whitney test). (b) Representative calcium response profiles

($\Delta F/F_0$) of A08n or Ln neurons after a 5 s red light pulse. (c) Mechano-nociceptive behavioral response of 3rd instar larvae at 96h AEL after the first (I) and second (II) mechanical stimulation with a 45 mN *von Frey* filament. *rTrpA1^{1}* mutant animals did not display nociceptive rolling or bending ($p<0.001$, chi^2 test). Silencing of C4da or A08n neurons with Kir2.1 strongly inhibited nociceptive rolling (n as indicated, $p<0.001$, chi^2 test). (d) Expression of CsChrimson in C4da, A08n or ilp7 neurons and induction of nociceptive rolling upon 5 s activation with 625 nm light (0.2 mW/mm^2, n as indicated, $p<0.001$, chi^2 test). (e) CsChrimson mediated C4da neuron activation while silencing A08n, ilp7 neurons or both with Kir2.1 results in significant reduction of nociceptive rolling (5 s activation, 625 nm, 0.2 mW/mm^2, n as indicated, $p<0.001$, chi^2 test).

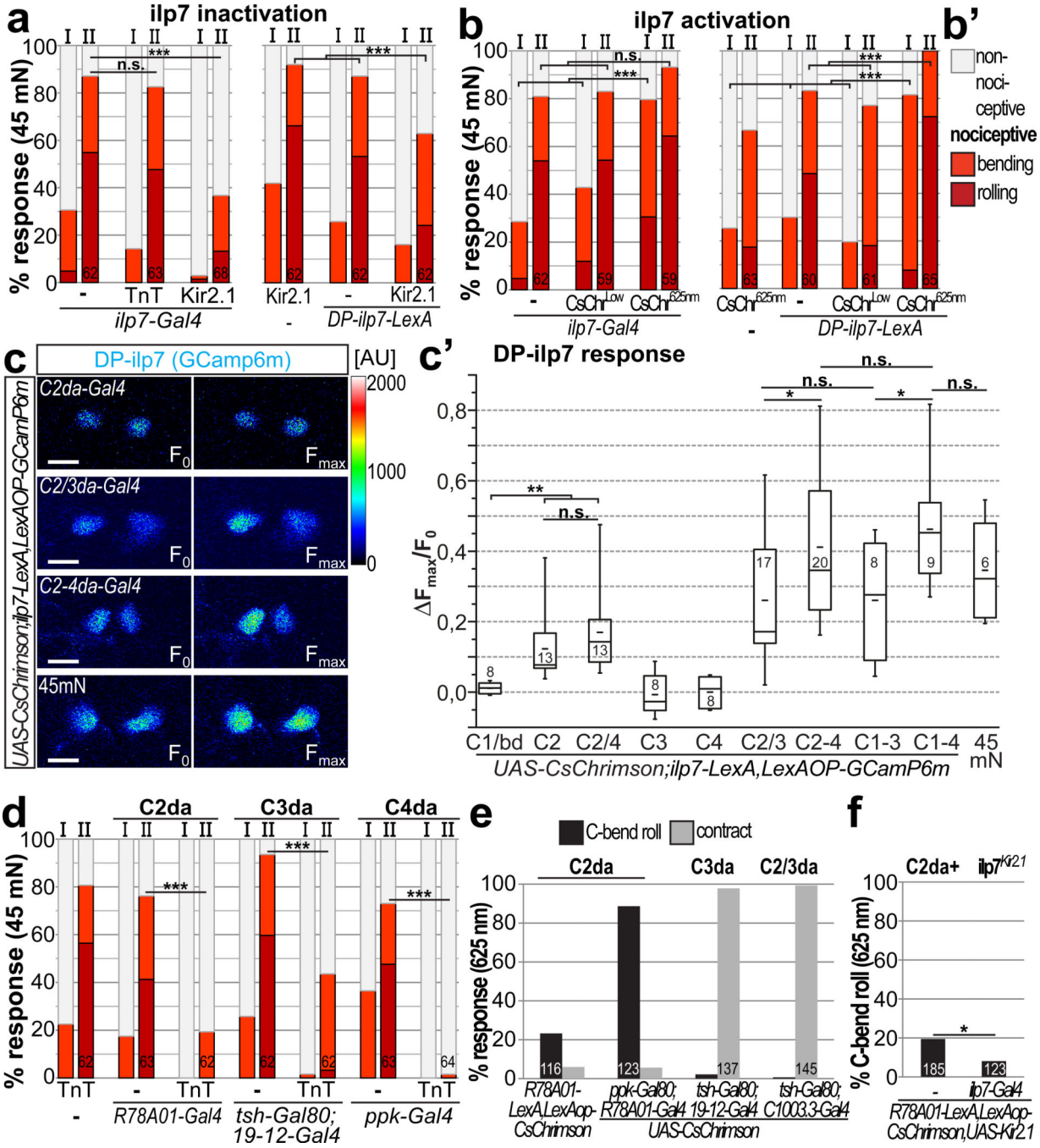

Figure 4. DP-ilp7 neurons integrate multi-mechanosensory input and facilitate nociceptive behavior

(a) Inactivation of ilp7 or specifically DP-ilp7 neurons with Kir2.1 but not TnT strongly inhibited nociceptive rolling after both stimuli (n as indicated, $p<0.001$, chi^2 test). (b) CsChrimson mediated acute activation of ilp7 or DP-ilp7 neurons during mechano-nociception. Expression of CsChrimson in ilp7 or DP-ilp7 neurons had no significant effect under low light conditions ($CsChrim^{Low}$) but strongly facilitated mechano-nociceptive behavior when activated with 625 nm light ($CsChrim^{625nm}$, 10 mW/mm^2, n as indicated, $p<0.001$, chi^2 test). (b') Legend for scored rolling, bending and non-nociceptive behavior for

(a,b,d). (c) Calcium responses of DP-ilp7 neurons expressing GCaMP6m using CsChrimson mediated optogenetic activation of C1da/bd (*2-21-Gal4*, n=8), C2da (*R78A01-Gal4*, n=13), C2/C4da (*R78A01/ppk-Gal4*, n=12), C3da (*nompC-Gal4*, n=8), C4da (*ppk-Gal4*, n=8), C2/C3da (*C1003.3-Gal4*, n=17), C2-4da (*C1003.3/ppk-Gal4*, n=20), C1-C3da (*21-7-Gal4, ppk-Gal80*, n=8), C1-C4da (*21-7-Gal4*, n=9) neurons or mechano-nociceptive stimulation with a 45 mN *von Frey* filament (n=6). (c') Maximum responses ($\Delta F_{max}/F_0$) were plotted and compared. Optogenetic activation of C2da neurons was sufficient to elicit calcium responses in DP-ilp7 neurons. DP-ilp7 responses scale with additional activation of C3da and C4da, but not C1da/bd neurons (C2/3da, C2-4, C1-C3da, or C1-C4da), similarly to mechano-nociceptive stimulation (45mn) (5 s activation, 625 nm, 0.2 mW/mm^2, *:p<0.05, **:p<0.01, Mann-Whitney test). (d) Mechano-nociceptive behavior of 3rd instar larvae at 96h AEL after the first (I) and second (II) mechanical stimulation with a 45 mN *von Frey* filament. TnT mediated silencing of C2da, C3da, or C4da strongly inhibits mechano-nociceptive responses (n as indicated, p<0.001, chi^2 test). (e) Optogenetic activation of C2da or C3da results in C-bend rolling or contraction behavior, respectively (5 s activation, 625 nm, 0.2 mW/mm^2). (f) C2da neuron dependent C-bend rolling is partially inhibited by ilp7 neuron silencing (5 s activation, 625 nm, 0.2 mW/mm^2, n as indicated, *:p<0.05, chi^2 test).

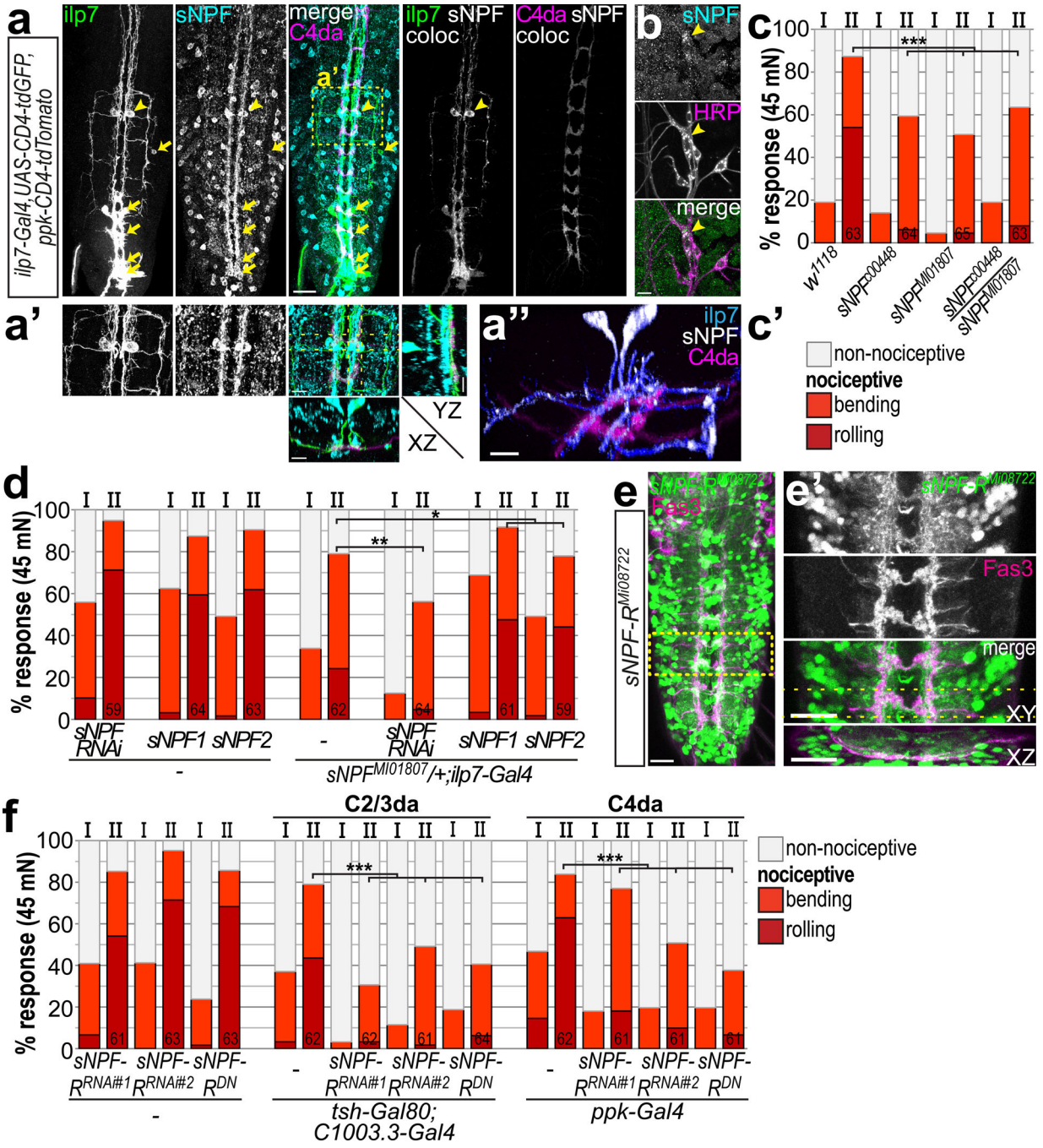

Figure 5. sNPF signaling from DP-ilp7 to mechanosensory neurons is necessary for mechano-nociceptive behavior

(a) DP-ilp7 and C4da neurons express sNPF. Anti-sNPF immunostaining and co-localization (coloc) with CD4-tdGFP expressing ilp7 or CD4-tdTomato labeled C4da axons. sNPF is expressed in DP-ilp7 (soma indicated by arrowheads) but not posterior ilp7 neurons (arrows). Scale bar: 50 μm (a') Enlarged view of boxed area in (a) and resliced maximal projections along the YZ and XZ axis (indicated by dotted lines) show that sNPF localizes to DP-ilp7 ventromedial and -lateral dendrites and C4da axon terminals. (a") 3D-view of boxed region (a'). Scale bars: 10 μm. (b) Body wall preparation showing specific anti-sNPF signal

in the C4da neuron soma (arrowhead), but not in other sensory neurons visualized with anti-HRP. Scale bar: 10 μm. (c) Mechano-nociceptive behavior of sNPF mutant 3rd instar larvae at 96h AEL. sNPF mutant alleles show mechano-nociceptive defects after mechanical stimulation with a 45 mN *von Frey* filament (n as indicated, $p<0.001$, chi^2 test). (b') Legend for scored rolling, bending and non-nociceptive behavior for (c,d). (d) Heterozygous *sNPF* mutant animals show reduced mechano-nociceptive behavior, which is further impaired by RNAi-mediated knockdown of sNPF in ilp7 neurons. Expression of sNPF1/2 in ilp7 neurons can significantly rescue mechano-nociceptive defects (n as indicated, $*p<0.05$,$**p<0.01$, chi^2 test). (e) Expression pattern of sNPF-R visualized by a GFP enhancer trap (*sNPF-R*^{Mi08722}) overlaps with sensory C2-4da neurons labeled by anti-Fas3. Scale bar: 50 μm. (e') Enlarged view of boxed area in (e) and maximal projections along the YZ and XZ axis (indicated by dotted lines). Scale bar: 10 μm. (f) RNAi-mediated knockdown of sNPF-R (*sNPF-R*^{RNAi}) or overexpression of a dominant negative transgene (*sNPF-R*^{DN}) in C2/3da or C4da neurons results in severe mechano-nociception defects (n as indicated, $p<0.001$, chi^2 test).

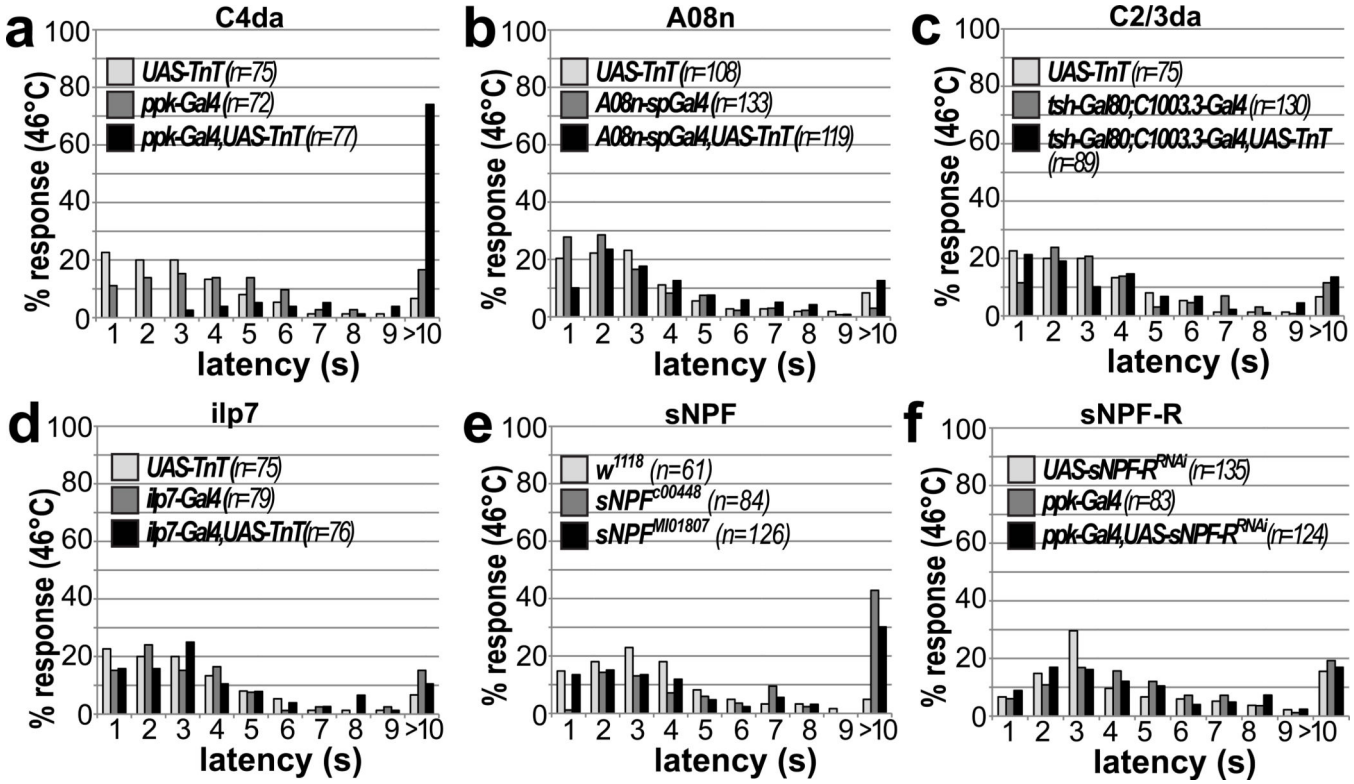

Figure 6. Mechano-nociceptive circuit elements and sNPF-R function are not required for C4da neuron dependent thermo-nociception

(a–d) Latency of nociceptive rolling responses was measured in 3rd instar larvae at 96h AEL after local simulation with a probe heated to 46 °C. TnT mediated silencing of different subsets of the nociceptive circuit confirms the requirement of (a) C4da neuron function (n as indicated, $p<0.001$, Kruskal-Wallis ANOVA, Dunn's *post-hoc* comparison). No thermo-nociceptive defects were observed when silencing (b) A08n, (c) ilp7 or (d) C2/3da neurons (n as indicated, $p>0.05$, Kruskal-Wallis ANOVA). (E) *sNPF* mutant alleles show a mild defect in thermo-nociception (n as indicated, $p<0.001$). (F) C4da neuron specific RNAi mediated knockdown of sNPF-R did not show significant differences compared to controls (n as indicated, $p>0.05$, Kruskal-Wallis ANOVA, Dunn's *post-hoc* comparison).

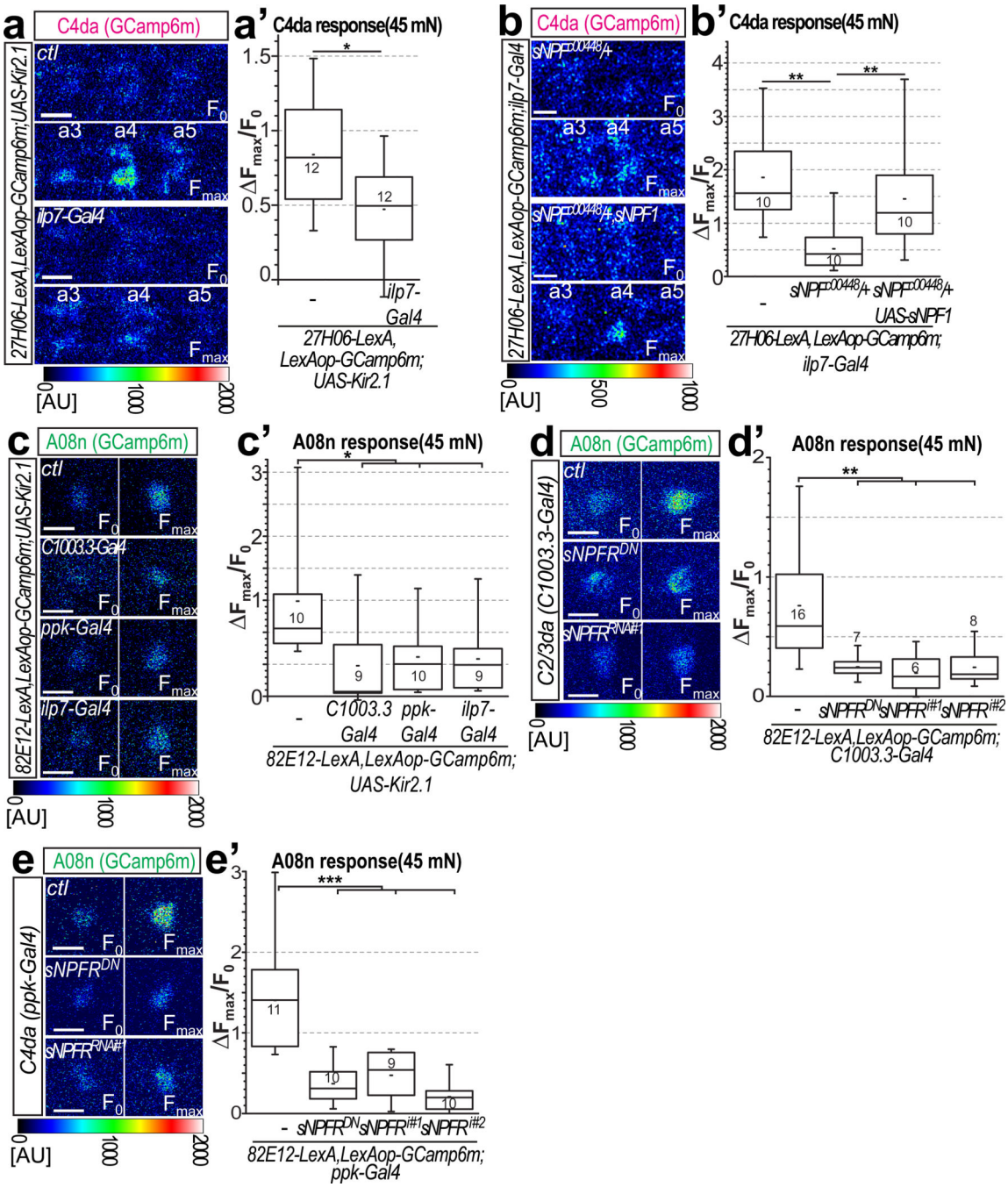

Figure 7. DP-ilp7 activity and sNPF signaling are required for C4da neuron presynaptic facilitation and A08n neuron responses

(a–b) Calcium responses visualized in C4da axon terminals expressing GCaMP6m after *von Frey* filament stimulation in semi-intact larval preparations. Baseline (F_0) and maximum responses (F_{max}) in C4da neuron terminals are shown for (a) control (ctl) and for ilp7 neuron inactivation by Kir2.1. Responses to local *von Frey* filament stimulation are restricted to a single VNC hemisegment corresponding to the stimulation site on the body wall. Scale bar: 10 μm. (a') Maximum responses ($\Delta F_{max}/F_0$) were plotted showing that ilp7 neuron inactivation reduces C4da neuron presynaptic calcium influx (n=12 each, $p<0.05$, Mann-

Whitney test). (b,b') Calcium responses in C4da axon terminals after mechanical stimulation are reduced in *sNPF* heterozygous animals and significantly rescued by sNPF expression in ilp7 neurons. (n=10 each, $p<0.05$, Mann-Whitney test). (c–e) Calcium responses in A08n somata expressing GCaMP6m (*82E12-LexA*) after mechano-nociceptive stimulation. (c) Baseline (F_0) and maximum responses (F_{max}) in A08n neurons are shown for control (ctl) and C2/3da, C4da, or ilp7 neuron specific inactivation by Kir2.1 expression. Scale bars: 10 μm. (c') Maximum responses ($\Delta F_{max}/F_0$) were plotted showing that A08n neuron calcium responses are strongly reduced upon inactivation of C2/3, C4da or ilp7 neurons (n=as indicated, $p<0.05$, Mann-Whitney test). (d,e) Baseline (F_0) and maximum responses (F_{max}) in A08n neurons are shown for control (ctl), RNAi mediated knockdown of sNPF-R and expression of a dominant negative sNPF-R in (d) C2/3da neurons or (e) C4da neurons. (d',e') Maximum responses ($\Delta F_{max}/F_0$) were plotted showing that inactivation of sNPF signaling in either sensory subset significantly impairs A08n neuron responses (n=as indicated, $p<0.05$, Mann-Whitney test).